EXPERIMENTAL DETERMINATION OF THE AVERAGE HEAT TRANSFER COEFFICIENT FOR YAW CYLINDERS

by

Marco Antonio Viteri

United States
Naval Postgraduate School

THESIS

EXPERIMENTAL DETERMINATION OF THE

AVERAGE HEAT TRANSFER COEFFICIENT

FOR YAW CYLINDERS

by

Marco Antonio Viteri

April 1969

EXPERIMENTAL DETERMINATION OF THE AVERAGE HEAT TRANSFER COEFFICIENT FOR YAW CYLINDERS

by

Marco Antonio Viteri
Lieutenant, Ecuadorian Navy
B.S., Chilean Naval Academy, 1960

Submitted in partial fulfillment of the
requirements for the degree of

MASTER OF SCIENCE IN MECHANICAL ENGINEERING

from the

NAVAL POSTGRADUATE SCHOOL
April 1969

ABSTRACT

The heat transfer characteristics of yawed cylinders was measured in an open induction tunnel in the subsonic range. Two model diameters were tested, 0.50 inches and 0.25 inches. The Reynolds number based on cylinder diameter was varied from 2750 to 33200 for the 0.50 inch diameter model and from 1430 to 16700 for the 0.25 inch diameter model.

The tests showed a good agreement for both models with the experimental results of other investigators for the normal case, or zero yaw case. As yaw angle was increased from the normal position to about 35 degrees, a peaking in the heat transfer was obtained. As yaw angle was increased further the average Nusselt number decreased. This behavior is attributed to the end effect of the models used whose aspect ratio were limited by the size of the test section. At larger yaw angles there is an agreement of the heat transfer data for models with similar aspect ratio.

TABLE OF CONTENTS

LIST OF TABLES

LIST OF ILLUSTRATIONS

NOMENCLATURE

English Letter Symbols

A_s	Model surface	ft^2
A_1, B_1	Constants in King's Law	
A_2, B_2	Constants in parallel cylinder heat transfer equation	
Bi	Biot Number, $(h\ D)/k_m$	
B, n	Constants in Hilpert's normal equation	
C_1, C_2	Constants in normal equation indicated by Richardson	
c	Specific heat of model material	Btu/(lbm °F)
D	Diameter of the model	in
g_c	Proportionality factor in Newton's Second Law, 32.174	(lbm ft)/(lbf sec^2)
h	Heat transfer coefficient	Btu/(sec ft^2 °F)
k	Thermal conductivity of air evaluated at film temperature	Btu/(sec ft °F)
k_m	Thermal conductivity of model	Btu/(sec ft °F)
K_1, K_2, K_3	Constants in Equations (D-4), (D-5) and (D-9) respectively	
L	Length of the model proper	in
L_a	Length of the model assembly from the leading edge to the holder piece	in
m	mass of the model	lbm
Nu	Nusselt Number, $(h\ D)/k$	
p	Manometric pressure	in-H_2O
P	Absolute pressure	lbf/ft^2

Re	Reynolds Number based on cylinder diameter, $(U\ D\ \rho)/\mu$	
t	Temperature	°F
T	Temperature	°R
T_f	Film Temperature, $(T + \bar{T}_w)/2$	°R
$\bar{T}_w$	Average wall temperature, $(\bar{T}w_{in} + \bar{T}w_{fin})/2$	°R
U	Air velocity	ft/sec

Greek Letter Symbols

Δ	Denotes difference	
ε	Emissivity of the model	
θ	Time	sec
Λ	Yaw angle, i.e., the angle between the spanwise axis of the model and the plane perpendicular to the free stream flow direction	deg
μ	Dynamic Viscosity of air evaluated at film temperature	lbm/(ft sec)
ρ	Mass density of air	lbm/ft^3
σ	Stefan-Boltzmann constant, 0.1714×10^{-8}	$Btu/(hr\ ft^2\ °R^4)$

Subscripts

b	Referred to model proper before assembly
d	Dynamic value
f	Property evaluated at the film temperature
s	stagnation (total) value
w	at wall of the model
in	initial value

fin	final value
H, M	referred to Hilpert and McAdams correlation for Reynolds Number respectively
∞	Free stream value

ACKNOWLEDGEMENTS

The author wishes to express his gratitude to Professor Paul F. Pucci for his continued support and encouragement during the course of this investigation. He also wishes to thank Professor Paul J. Marto for his constructive criticism as Departmental Reader.

A special note of appreciation is given to Messrs. K. Mothersell and J. McKay for their efforts in the construction of the experimental apparatus.

1. Introduction.

The problem of the forced convection heat transfer in flows normal to cylinders has been investigated since the early workers in the field of the hot wire anemometry. The mathematical description of the rate of heat transfer as a function of the air velocity was first presented in 1914 by Professor L. V. King [1][1]. The relation, King's Law, has the form

$$Nu = A_1 + B_1 Re^{0.5}$$

The form of this relation was subsequently found to be correct for wide ranges of Reynolds numbers and is particularly accurate in the velocity range from 0 to 300 feet per second for ordinary hot wires. The heat transfer from a hot wire thus varies with the square root of the wire Reynolds number if the temperature and composition of the fluid remain constant. King also measured a reduction of heat transfer by yawing the cylinder axis from normal to the flow direction.

McAdams [2] presents the data of Hilpert, which includes cylinders with diameters of 0.0079 to 5.9 inches normal to the flow direction, together with a recommended curve relating the Nusselt number with the Reynolds number. The entire range of data is segmented into portions correlated by equations in the form $Nu = B\ Re^n$. Table 10-3 of reference [2] gives the value of the coefficient B and the exponent n for several ranges of Reynolds numbers. Hilpert's data are the backbone of the present normal correlation.

[1]Numbers in brackets refer to numbered items listed in references.

Squire, cited by Schmidt and Wenner [3], presents a theoretical solution at the forward stagnation point of a cylinder. The data obtained by Schmidt and Wenner verified precisely Squire's correlation as $Nu = 1.01\ Re^{0.5}$.

Baldwin, Sandborn and Laurence [4], presented a summary of the data for the normal case in the continuum, slip, and free moleculae air flows. Giedt [5] investigated the effect of turbulence of the incident air stream on local heat transfer on a cylinder.

The effect of sweep-back on the heat transfer has been largely investigated, because of its application in the flight of aircraft and missiles, at supersonic speeds. Blunting the leading edges of wings reduces the local increase in heat transfer, but increases the drag. However, if the leading edge is swept back, the heat transfer rate due to the leading edge is reduced below that occurring if the leading edge is normal to the direction of flight and also the drag due to the blunted leading edge is reduced. References [6] and [7] investigated the effect of yaw on the heat transfer coefficient at supersonic speeds.

The yawed infinite cylinder simulates approximately the leading edge of a swept-back wing and allows a basic simplification of the boundary layer theory. Sears [8] and other investigators observed that for incompressible flow over a yawed infinite cylinder the boundary layer development in the chordwise direction (normal to the cylinder axis) is independent of the spanwise flow. For compressible flow, however, this independence principle does not apply.

Where the independence principle applies, the solutions for the boundary layer development in the chordwise plane are those which have been obtained for incompressible two dimensional flow. Sears presented

a series type solution to the spanwise velocity gradient distribution around a cylinder. It was noted [8] that in a steady, incompressible flow the distribution of spanwise velocity is the same as the distribution of temperature when the cylinder surface is maintained at a uniform temperature different from the stream temperature, provided that the Prandtl number is unity and viscous heating is neglected. Based on this, Goland [9] showed that in an incompressible fluid of Prandtl number unity the heat transfer of a yawed cylinder varies as the square root of the Reynolds number based on the normal component of the stream velocity. Thus, for a given stream velocity, the heat transfer coefficient decreases as the square root of the cosine of the yaw angle. This decrease is associated with the increase in boundary layer thickness due to yaw.

The fact that yawing of cylinder reduces the average heat transfer coefficient has been shown by workers in hot wire annemometry. Reshotko [10] and Reshotko and Beckwith [11] gave a solution of the compressible laminar boundary layer equations at the stagnation line of yaw cylinders. For Mach numbers from 0 to 0.5 they found that the effect of yaw can be accounted for by writing Nusselt number as a function of the square root of the product of the Reynolds number and the cosine of the yaw angle. Thus, for incompressible flow the theoretical variation of the ratio of the stagnation line heat transfer for yawed infinite cylinders to the stagnation line heat transfer coefficient at zero yaw reduces to

$$\frac{h_{\Lambda}}{h_{\Lambda=0}} = (\cos \Lambda)^{0.5}$$

where Λ is the angle of yaw, i.e., the angle between the spanwise axis of the model and the plane perpendicular to the free stream flow direction.

Thus a cylinder normal to the flow is at zero yaw, while the yaw angle for a cylinder parallel to the flow is 90 degrees. This was obtained experimentally with hot wires by Schubauer and Klebanoff [12]. The Reshotko and Beckwith laminar theory cannot be applied to large yaw angles, since the initial hypothesis in the development of the theory that the spanwise derivatives are identically zero does not apply. Based on Reshotoko and Beckwith investigation, Baldwin, Sandborn and Laurence [4] indicated that for yaw angles between 0 to 70 degrees, the use of the correlation of convective heat transfer for transverse cylinders, that they presented in their Figure 6, with Re CosΛ instead of Re, should give a good engineering estimate of the heat transfer for yawed cylinders for Re CosΛ $>$400 in subsonic flow.

Schubauer and Klebanoff [12] suggest that the yaw data could be correlated by the normal Reynolds number as

$$Nu = A_1 \ (Re \ Cos \ \Lambda)^{0.5} + B_1$$

Sandborn and Laurence [13] indicated that in general this correlation is adequate only near zero Mach number and angles of yaw less than 70 degrees. They correlated their data for all yaw angles within approximately ten percent with an equation of the form

$$Nu = [A_1 \ (Re \ Cos \ \Lambda)^{0.5} + B_1] \ Cos\Lambda + [A_2 (Re \ Sin\Lambda)^{0.5} + B_2] \ Sin\Lambda$$

obtained by combining the heat loss of wires normal and parallel to the flow. However, they found systematic variations rather than random, indicating a need for a still more accurate equation.

The object of the present investigation was thus to determine experimentally the heat transfer characteristics of yawed cylinders for yaw angles 0 to 90 degrees in the Reynolds number range 1500 to 33000.

2. Description of the Equipment.

a. Wind tunnel.

The tests were performed in an open induction tunnel shown in Figure 1. The suction side of four feet square is covered with a fine screen to reduce large scale turbulence. The settling section is two feet long with a cross sectional area of one square foot.

A nozzle with a contraction ratio 6:1 connects the upstream side to the test section. An eight foot long duct connects the test section downstream to the suction side of a fan propelled by a 0.75 HP AC electric motor. A gate valve at the exit of the fan controls the mass flow rate.

b. Test section.

The plastic test section is two feet long and has a rectangular cross section of four by six inches. Figure 2 shows the test section. Two circular openings were made on the ceiling. The first one, located 8.5 inches from the upstream flange, was used to locate a 0.25 inch Flow Corporation pitot-static tube to measure the free stream velocity. This will be referred to as station No. 1 or the upstream station. The second opening, seven inches downstream of the first, was used to locate the models for the heat transfer tests. This will be referred to as station No. 2 or the downstream station. The center of this station is located 1.75 inches from the nearest lateral wall in order to perform the tests for all yaw angles from 0 to 90 degrees, that is, changing the position of the models from a normal position with respect to the flow, to the parallel position.

A plastic circular cover with a small hole for the location of the pitot tube was used at station No. 1. A similar cover was used at

station No. 2 to be placed instead of the model assembly during the time when the model was heated outside the test section. Two quick action spring locks press the covers against the test section ceiling to minimize leakage. Static pressure taps were placed in the side and bottom walls.

c. Models.

A protractor from a drafting machine mounted in a six inch circular plastic piece, was used to locate the models at the desired yaw angle in a fast way and with an accuracy estimated of the order of one degree.

Two models were used for the present tests. The first is a 0.50 inch diameter cylinder shown in Figure 3. A 0.50 inch diameter stainless steel holder piece was mounted in the protractor. The model was made using three similar copper cylinders 0.75 inches long and separated by small bakelite insulating cylinders 0.1875 inches long.

A special technique was used to get a uniform model without discontinuities and good finished surfaces. The bakelite cylinders were made of larger diameter and with the ends like rings to hold the copper cylinders in the correct position allowing a good alignment. The cylinders were bonded together using epoxy adhesive. After drying, the assembly of cylinders was machined down to 0.50 inches diameter.

The copper cylinder near the holder piece and the bakelite insulators located at its sides have a 0.062 inch diameter hole in the center to allow the passage of a 30-gage copper-constantan thermocouple wire to the boundary of the center solid copper cylinder or the model proper. The basic idea of this design of the model, using the two copper cylinders similar to the model proper at its sides is to minimize the effect of conduction in the axial direction. Figure 6 shows a sketch of the 0.50 inch model.

The length of the model was governed by the width of the test section. As the yaw angle was increased, longer models were possible. This was accomplished by replaceable bakelite sections which were attached.

Three removable extension pieces were used. One 0.656 inches long was used in the 30 and 40 degree yaw position, one 1.469 inches long in the 50 degree position and one 3.969 inches long in the 60 to 90 degree positions.

The second model shown in Figure 4, is similar to the first but 0.25 inches in diameter, all the other dimensions being the same.

d. Heater.

The heater was made by coiling a 18-gage, nichrome wire covered with ceramic bead insulators around a steel cylinder. A second steel cylinder was placed concentrically around the heater coil and covered with asbestos tape. Both heater ends were covered with insulation to decrease the heat losses. Openings of 1.25 inches diameter were made, to allow the passage of the models to a position in which the model proper was in the center of the heater. A wooden frame supports the protractor mount during the heating.

The power was supplied by a Powerstat variable transformer. The current and voltage required for the heater were measured by Weston AC meters.

e. Instrumentation.

Figure 5 shows the general disposition of the instrumentation.

1. Manometers.

A manometer board with a set of Ellison inclined and vertical manometers was used for the pressure measurements. The accuracy of these manometers is within one half percent of the full scale.

The following manometers were used:

(1) Ellison inclined manometer, 0-0.2", smallest division 0.001".

(2) Ellison inclined manometer, 0-2", smallest division 0.005".

(3) Ellison inclined manometer, 0-4", smallest division 0.010".

(4) Ellison inclined manometer, 0-12", smallest division 0.020".

(5) Ellison vertical manometer, 0-17", smallest division 0.100".

(6) Ellison vertical manometer, 0-36", smallest division 0.100".

2. Thermocouples.

Thermocouples were made from 30-gage copper-constantan wire. The junctions for the model and for the free stream temperatures were first calibrated with a Leeds and Northrup precision potentiometer with ice and steam as the reference temperature. The free stream thermocouple junctions were located 22 inches upstream of the test section.

3. Recorder.

The temperature difference between the model and the

free stream was registered during the experiments using a 7100B Hewlett Packard strip chart recorder with plug-in 17500/A.

The free stream temperature was measured for each test with a Leeds and Northrup portable potentiometer with an ice reference.

3. Experimental Procedure.

a. Test section calibration.

The test section was calibrated without the models. The velocity profile was determined at the two stations of the test section by a traverse with the pitot tube in both vertical and horizontal directions. At the same time static pressures were measured at station No. 1 and at the pressure taps corresponding to the position of the model at station No. 2.

The velocity was found to be practically uniform across the tunnel test section to within 0.25 inches of the wall. Comparison of the velocity measured with the pitot tube and that evaluated by static wall pressure measurements, indicated that the velocity could be evaluated using the pitot static tube with a stagnation point pressure coefficient of 1.0. Velocities from 11 to 145 feet per second were measured at station No. 2.

b. Heat transfer experiments.

The models were carefully polished before each run to minimize radiation losses. The Powerstat was set for an output to the heater of 11 volts. The heater was maintained operating at a constant current of 4.5 amperes.

The millivolt potentiometer was standardized before each run. The strip chart recorder was calibrated by supplying a voltage of one millivolt from the potentiometer. This was done first at the one millivolt scale of the recorder and then at the two millivolt scale.

Before each run the atmospheric pressure indicated by a Princo Fortin Type barometer was observed. The free stream temperature was

measured for each run by a thermocouple and the portable potentiometer and also by a mercury thermometer located at the inlet of the tunnel.

The tunnel was set at the desired velocity by adjusting the control valve. Once the conditions of steady flow were met, the model was removed from the test section and placed into the heater. A plastic cover was used to replace the protractor-model assembly.

The models were heated to about 65 to 105 degrees above ambient temperature, corresponding to a difference of 1.5 to 2.5 millivolts of thermocouple output. It took about twenty minutes for the heater interior steel surface to reach a temperature of about 250 degrees Fahrenheit. The heating process was accomplished by free convection and radiation. It took about five minutes to heat the 0.50 inch model to 140 degrees Fahrenheit and about three minutes to heat the 0.25 inch model to 150 degrees.

Once the desired model temperature was reached, the model was removed from the heater and positioned in the test section. The plastic cover piece of the model assembly was quickly fastened by the two lateral spring locks. The model was placed in the desired yaw angle using the protractor mechanism.

The temperature of the model during the initial phase of the cooling process was monitored by the recorder on the five or two millivolt scales as convenient. Just before a temperature difference corresponding to 1.0 mv. was reached, the recorder scale was set at this value and the temperature-time history of the model initiated at a conveniently selected chart speed. Figure 7 shows a typical model cooling record.

The manometers were observed during the cooling of the model and the readings noted when the temperature difference between the model and

the free stream indicated by the recorder was about 0.6 millivolts. In general the manometer fluctuations during the tests were small. Negligible fluctuations were observed at the low and medium Reynolds number runs for both models. At the higher velocity runs, fluctuations of the order of 1.5 to 2.0 percent of the reading were observed.

Ten series of runs at different flow rates were made with the 0.50 inch model. Seventeen runs were made at each flow rate with this model. The first ten runs were made using the basic model without additional cylinder extensions at the end. These runs were performed for each ten degrees of yaw angle from 0 to 90 degrees. Another seven runs were made using the additional cylinder extensions.

The procedure followed in the individual runs with the 0.25 inch model was the same except that only nine mass flow rates were used. Some vibration was detected during the two higher speed runs with this model using the largest extension.

The pitot static tube was located 0.5 inch from the upper wall of the test section to avoid disturbances in the flow upstream of the model. For the runs with the 0.50 inch model the upstream velocity changed from 11 to 136 feet per second. The corresponding changes in Reynolds number was from 2750 to 33200. For the 0.25 inch model the velocity changed from 12 to 138 feet per second. The corresponding change in Reynolds number was from 1430 to 16700.

It was noted that by changing the yaw angle of the 0.50 inch diameter model from the normal to parallel position, the air velocity increased about five percent at high flow rates, decreasing to about one percent at the low flow rates. However, for the 0.25 inch diameter model the increase in local velocity is less than two percent at high flow rates.

4. Presentation of Results.

The experimental data is given in both tabular and graphical form. Tables III and IV give the heat transfer data for the 0.50 inch and 0.25 inch models respectively. Figure 9 is a summary of the normal heat transfer data for both models. Hilpert's correlation, mentioned by McAdams [2], and data from Schmidt and Wenner [3] is also plotted for comparison purposes.

Figure 10 shows the average Nusselt number versus Reynolds number correlated in two ways for the 0.50 inch model at 20 degrees yaw.

Figures 11 through 13 show the average Nusselt number versus Reynolds number for both models at yaw angles 30, 50, and 60 degrees respectively. Figure 14 shows the parallel heat transfer data for both models.

The experimental variation of the average Nusselt number for the yawed cylinder to the average Nusselt number of the cylinder at zero yaw at representative Reynolds numbers is given in Figures 15 through 17 for the 0.50 inch model and in Figures 18 through 20 for the 0.25 inch model.

5. Discussion of Results.

a. Normal case.

Figure 9 presents a comparison of the data obtained at zero yaw for both models. Hilpert's correlation cited by McAdams [2] and the data of Schmidt and Wenner [3] are also shown.

In general the present experimental points lie above Hilpert's correlation, the maximum deviation being about 18 percent at the low Reynolds numbers decreasing to about two percent at the higher Reynolds numbers. The average of local measurements made on big cylinders by Schmidt and Wenner lie above the present experimental points and also above Hilpert's correlation. The maximum difference between Schmidt and Wenner experimental averages and the present tests is of the order of 13 percent. Schmidt and Wenner explained the fact that their data lie above Hilpert's correlation to inevitable and greater measuring errors in the experimental method that they used.

A correlation in the form suggested by Richardson [14] was obtained for the two models in normal flow. The mean heat transfer coefficient for a cylinder can be estimated as the sum of the contributions from the forward boundary layer and from the rearward separated regions. At Reynolds numbers for which an attached turbulent boundary layer is absent, the mean transfer coefficient can be written as

$$Nu = C_1 \ Re^{1/2} + C_2 \ Re^{2/3}$$

The graph of the mean heat transfer, as $\frac{Nu}{Re^{1/2}}$, against $Re^{1/6}$ gives a straight line of slope C_2 and intercept C_1. The correlation thus obtained for the present normal tests for $1400 < Re < 33200$ is

$$Nu = 0.400 \ Re^{1/2} + 0.354 \ Re^{2/3}$$

with a maximum deviation of eight percent.

The intercept obtained is in agreement with the expected value from the boundary layer theory. The slope is within four percent of the value given by Jakob and Hawkins [15] as the average from measurements of different investigators.

b. Yawed cylinders.

Reshotko and Beckwith [11] give a solution of the compressible laminar boundary layer equations at the stagnation line of yawed cylinders. For Prandtl number equal to one and the incompressible flow case their solution indicates that the ratio between the heat transfer coefficient at an angle of yaw to the normal (zero yaw) heat transfer coefficient at the stagnation line is equal to the square root of the cosine of the yaw angle. This theoretical solution is also shown in Figures 15 through 20 for comparison with the present experimental data at different yaw angles, for both the basic model and for the model with extensions.

The decrease in the average heat transfer coefficient for the models with extensions is apparent from the figures. The reason is due to the greater aspect ratio L_a/D of the models with additional cylinders. These more nearly approach the ideal case of an infinite long cylinder, the basic assumption of the theory. The length of the models of the present tests was limited by the width of the tunnel test section. Table I presents the aspect ratios of the models for the different yaw angles. The aspect ratio is considerably smaller than the 0.5 inch diameter 24.0 inches long copper model used by Bechwith and Gallagher [7].

The data obtained from the 0.25 inch model is closer to the laminar theory because the aspect ratio for this model is twice that of the 0.50 inch diameter model.

The trend of the data is better shown in Figures 15 through 20 which present the ratio of the average Nusselt number at a given yaw angle to the average Nusselt number at zero yaw, as a function of yaw angle for a particular approach Reynolds number. Also shown is the theoretical laminar solution from Reshotko and Beckwith [11].

For the 0.50 inch diameter basic model, increasing the yaw angle from 0 to 35 degrees, the average heat transfer coefficient increases by about 26 percent at a Reynolds number of 31900, see Figure 17. This trend is different from that indicated by the laminar theory and which was obtained experimentally for wires by Schubauer and Klebanoff [12]. Sandborn and Laurence [13] observed a heat transfer coefficient at 35 degrees that was about ten percent lower than the values at zero yaw.

Further increase in yaw angle from 35 to 70 degrees results in a reduction in the average heat transfer coefficient of the 0.50 inch basic model of about 24 percent from the peak values. The trend of the experimental data obtained at other Reynolds numbers with this model is similar, see Figures 15 and 16. In general at lower Reynolds numbers the peaking values are smaller. The reduction in average heat transfer coefficient for the tests with the extensions is indicated in these figures.

The data obtained from the 0.25 inch model shows a similar trend with an increase in the average heat transfer coefficient of about 12 percent at a yaw angle of 30 degrees at a Reynolds number of 9050, see Figure 20. An increase in the yaw angle to 70 degrees results in a decrease of about 38 percent from the peak value. The percent of increase in the average heat transfer coefficient at the peak value is smaller for the 0.25 inch model than for the 0.50 inch model. The maximum increase in the average heat transfer coefficient for the 0.25 inch

model with the extensions is about the same percent as the basic model, see Figures 18 through 20. The peak in average heat transfer is at about the same yaw angle. At larger yaw angles the reduction in heat transfer coefficient of the models with the extensions is greater because of the larger aspect ratio.

The trend for both models is similar to that obtained for Beckwith and Gallagher [7] in supersonic flow. They explained their results by a phenomena of transition from laminar to turbulent boundary layer. This transition apparently occurred primarily as a result of a dynamic type of instability which is associated with the secondary flow in the boundary layer. The same agrument cannot be used to explain the trend of the present tests, because the range of Reynolds numbers is well below the values indicated by Owen and Randall, mentioned in [7], for the transition from laminar to turbulent as a result of secondary flow that occurs within the boundary layer on a yawed cylinder. It is interesting to note that the Reynolds number for the transition phenomena described by Owen and Randall decreases with yaw angle. Burnsnall and Loftin, mentioned in [7], observed a decrease in the stream Reynolds number for transition on circular cylinders (Re_T), from 3.7×10^5 to 2.1×10^5 for an increase in yaw angle from 0 to 60 degrees. Furthermore, the experimental transition Reynolds number obtained by Scott-Wilson and Caps, mentioned in [7], was about one tenth of the value predicted by the criterion of Owens and Randall. Being the trend of the data obtained similar to that of Beckwith and Gallagher [7], however, the peak values obtained in the present tests are well below those obtained by them. The maximum deviation from the value predicted by the laminar theory for the 0.50 inch model is about 44 percent, and is about 24 percent for the 0.25 inch model. The use of finite

length cylinder with an exposed end is the departure from the infinite length idealization of the theory. The pattern of the flow is changed from that corresponding to an infinite yaw cylinder, due to the end effect of the model. The decrease in heat transfer coefficient obtained for the tests with the extensions was less than expected for the corresponding increase in the aspect ratio. The heat transfer characteristics of the models used in the present tests seems to be influenced by the end effect whose intensity depends upon the distance from the model proper to the leading edge and the yaw angle. This effect takes place as soon as the model is given a small yaw angle. For a given model at a given yaw angle the heat transfer coefficient decreases by increasing the distance from the leading edge to the model proper. For a model of a given aspect ratio the influence of the end in the flow past the cylinders increases with the yaw angle. At low yaw angles, the large aspect ratio of the 0.25 inch model resulted in values closer to the predicted than the lower aspect ratio of the 0.50 inch model. At large yaw angles the influence of the aspect ratio in the intensity of the end effect can be seen by comparing the heat transfer data of the 0.5 inch model with the larger extension with that of the 0.25 inch basic model both of which have about the same aspect ratio. The data for these two models is approximately the same. Change in aspect ratio results in a departure from this observed agreement.

c. Parallel case.

The flow geometry for this case becomes completely different from the previous cases. The influence of the aspect ratio in the intensity of the end effect can be appreciated in this limiting situation. A big difference in the heat transfer data for models with different aspect ratio can be noted. The agreement in the heat transfer data for

models with similar aspect ratio is seen in Figure 14. Thus data for the 0.50 inch model with the larger extension and the data for the 0.25 inch basic model can be correlated in the form indicated by Sandborn and Laurence [13] by $Nu = 0.48\ Re^{0.5}$, with a maximum deviation of about 12 percent.

6. Conclusions.

The tests showed a good agreement with the experimental results of other investigators for the normal or zero yaw case.

The peaking in the heat transfer coefficient obtained at a yaw angle of about 35 degrees is attributed to the end effect of the models used whose aspect ratios were limited by the size of the test section. This end effect causes a change in the flow pattern with respect to that of an infinite cylinder.

For large yaw angles the agreement of the heat transfer data obtained for models with similar aspect ratio is apparent.

BIBLIOGRAPHY

1. King, L. V., "On the Convection of Heat from Small Cylinders in a Stream of Fluid," Philosophical Transactions of the Royal Society, London, Ser. A, v. 214, p. 373-432, 1914.

2. McAdams, W. H., Heat Transmission, p. 252-261, McGraw-Hill, 1954.

3. National Advisory Committee for Aeronautics, Technical Memorandum NACA TM 1050, Heat Transfer over the Circumference of a Heated Cylinder in Transverse Flow, by E. Schmidt and K. Wenner, 1943.

4. Baldwin, L. V., Sandborn, V. A., and Laurence, J. C., "Heat Transfer from Transverse and Yawed Cylinders in Continuum, Slip, and Free Molecule Air Flows," Journal of Heat Transfer, v. 82, p. 77-86, May 1960.

5. Giedt, W. H., "Effect of Turbulence Level on Incident Air Stream on Local Heat Transfer and Skin Friction on a Cylinder," Journal of the Aeronautical Sciences, v. 18, p. 725-730, November 1951.

6. National Advisory Committee for Aeronautics, Research Memorandum NACA RM A55H31, Investigation of Local Heat Transfer and Pressure Drag of a Yawed Cylinder at Supersonic Speeds, by G. Goodwin, M. O. Creager, and E. L. Winkler, January 24, 1956.

7. National Advisory Committee for Aeronautics, Research Memorandum NACA RM L56E09, Experimental Investigation of the Effect of Boundary Layer Transition on the Average Heat Transfer to a Yawed Cylinder in Supersonic Flow, by I. E. Beckwith and J. J. Gallagher, July 13, 1956.

8. Sears, W. R., "The Boundary Layer of Yawed Cylinders," Journal of the Aeronautical Sciences, v. 15, p. 49-52, January 1948.

9. Goland, L., "A Theoretical Investigation of the Heat Transfer in the Laminar Flow of Airfoils," Journal of the Aeronautical Sciences, v. 17, p. 436-440, July 1950.

10. Reshotko, E., "Heat Transfer to a Yawed Cylinder in Compressible Flow," Proceedings of the Heat Transfer and Fluid Mechanics Institute, p. 205-220, Stanford University Press, June 1956.

11. National Advisory Committee for Aeronautics, Technical Note NACA TN 3986, Compressible Laminar Boundary Layer over a Yawed Infinite Cylinder with Heat Transfer and Arbitrary Prandtl Number, by E. Reshotko and I. E. Beckwith, June 1957.

12. National Advisory Committee for Aeronautics, Report NACA WR W-86, Theory and Application of Hot Wire Instruments in the Investigation of Turbulent Boundary Layers, by G. B. Schubauer and P. S. Klebanoff, 1946.

13. National Advisory Committee for Aeronautics, Technical Note NACA TN 3563, Heat Loss from Yawed Hot Wires at Subsonic Mach Numbers, by V. A. Sandborn and J. C. Laurençe, July 12, 1955.

14. Richardson, P. D., "On Hilpert's Measurements of Heat Transfer from Cylinders Transverse to an Air Stream, "Journal of Heat Transfer, v. 85, p. 283-284, August 1963.

15. Jakob, M., and Hawkins G. A., Elements of Heat Transfer and Insulation, p. 115, Wiley, 1950.

16. Collins, D. C., and Williams, M. J., "Two Dimensional Convection from Wires Heated at Low Reynolds Numbers, "Aeronautical Research Laboratories, Australia, p. 357-361, March 1959.

17. Eckert, E. R. G. Heat and Mass Transfer, p. 513-514, McGraw-Hill, 1959.

18. National Bureau of Standards Circular 564. Properties of Air. 1955.

19. Kline, S. J., and McClintock, F. A., "Uncertainties in Single Sample Experiments," Mechanical Engineering, v. 75, p. 3-8, January 1953.

20. Modern Plastics Encyclopedia Issue for 1965. v. 42, Plastics Properties Chart Part II: Thermosets.

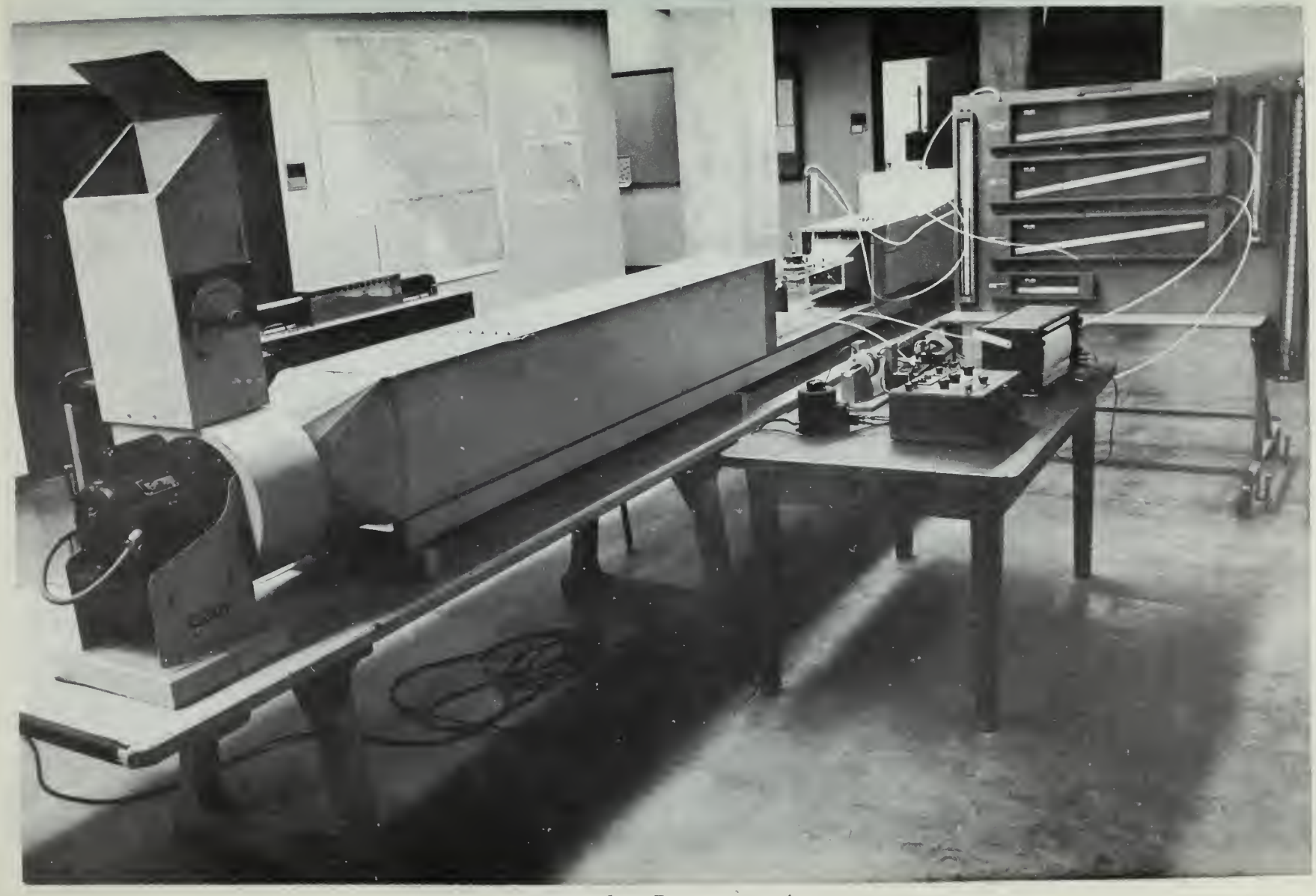

Figure 1. Test apparatus

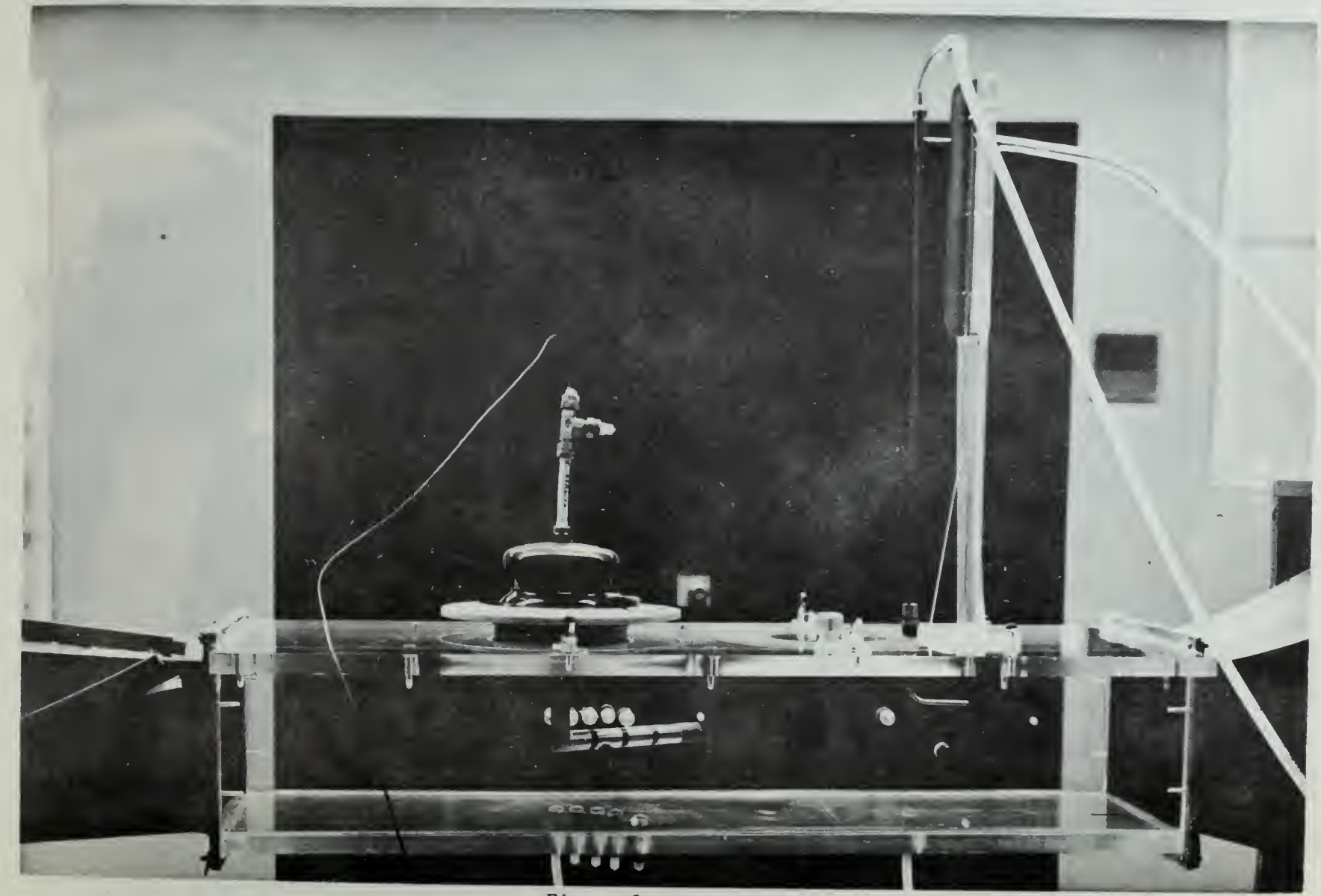

Figure 2. Test section

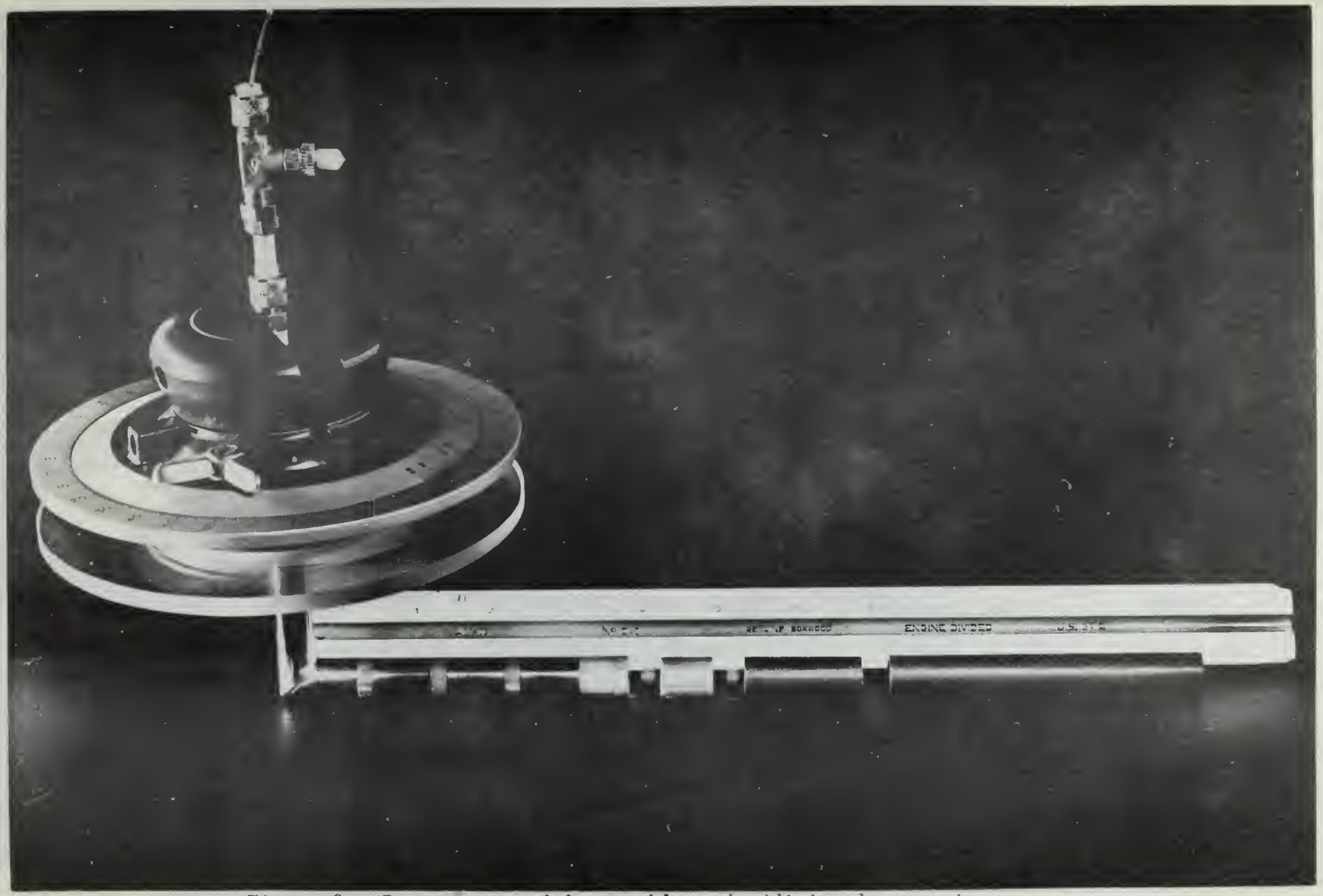

Figure 3. Protractor model assembly and additional extensions. Diameter: 0.50 inches.

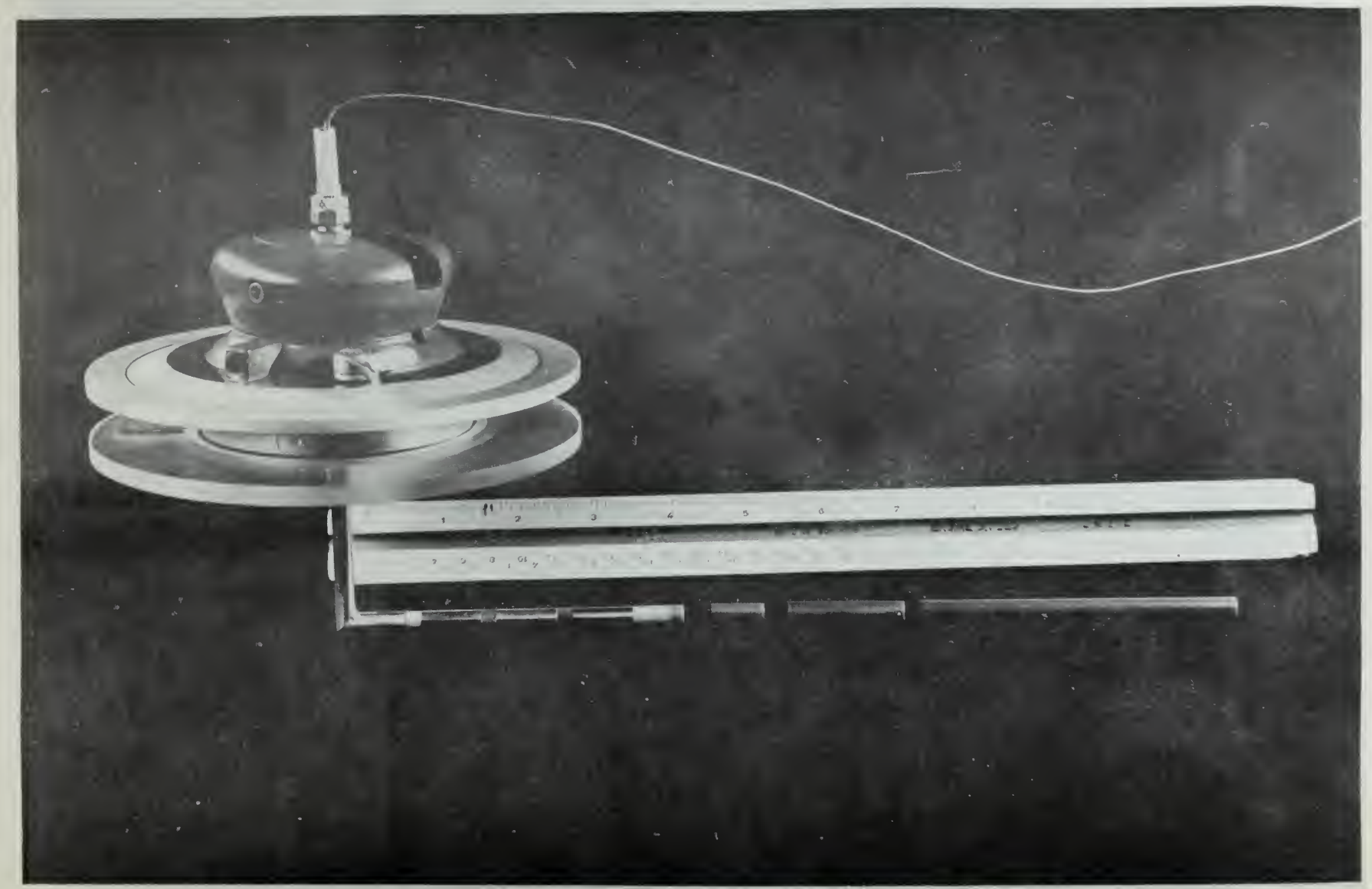

Figure 4. Protractor model assembly and additional extensions.
Diameter: 0.25 inches.

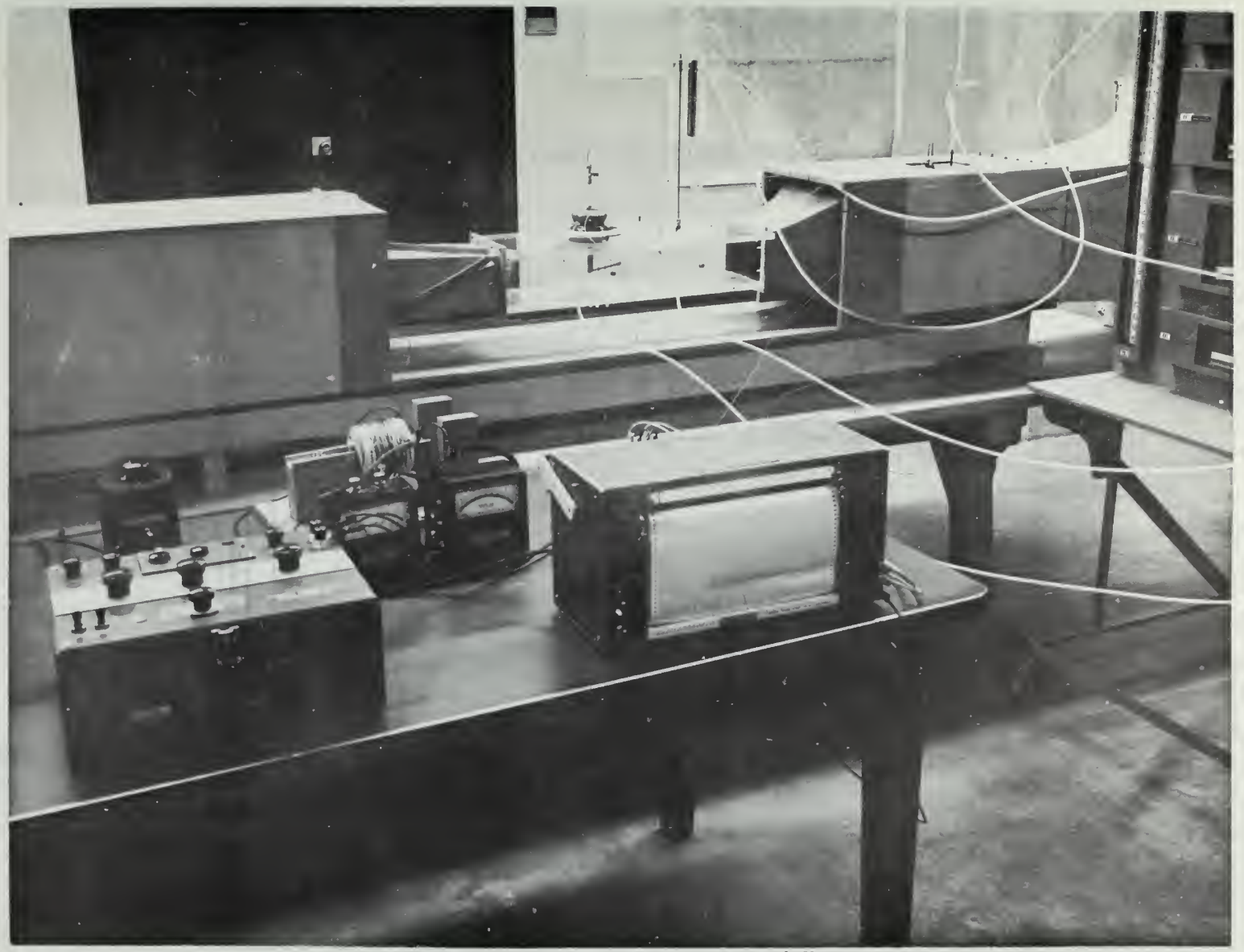

Figure 5. Instrumentation and Heater

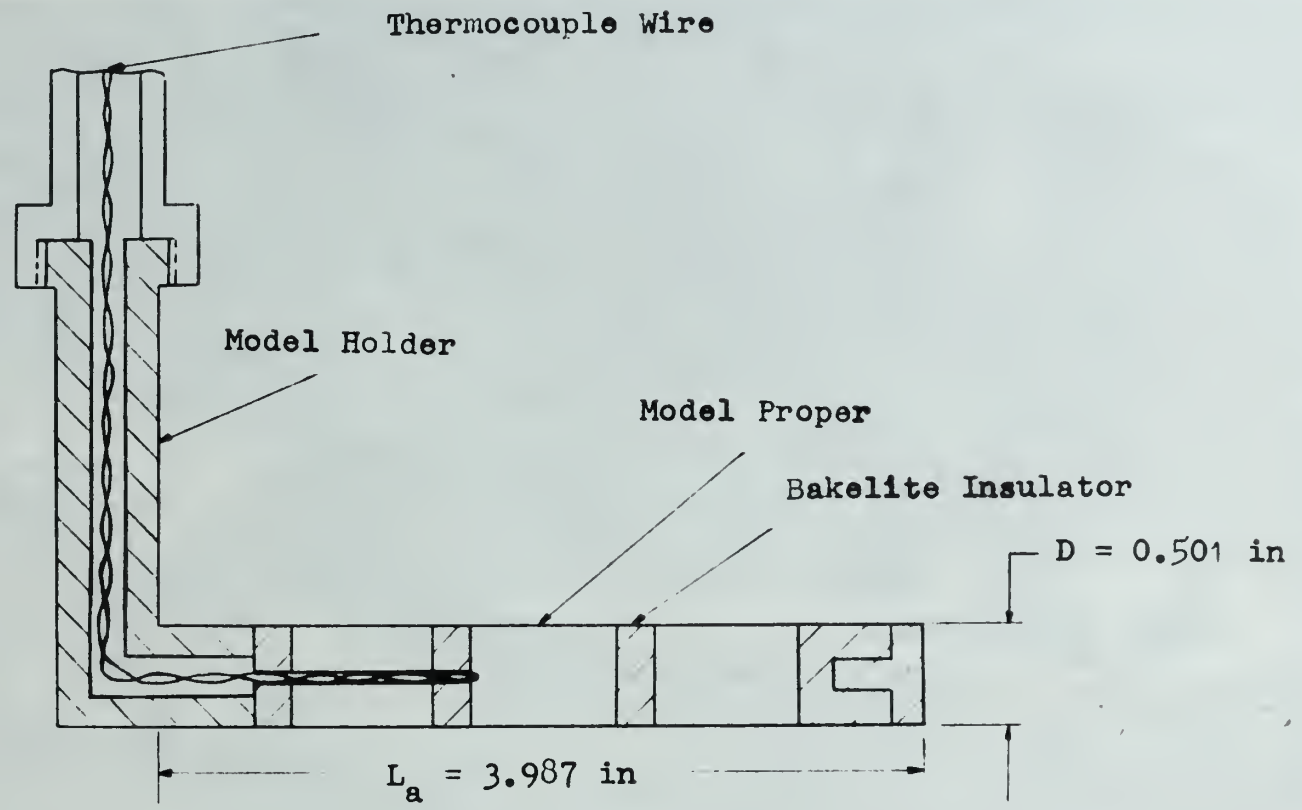

Figure 6. Sketch of the 0.50 inch Model

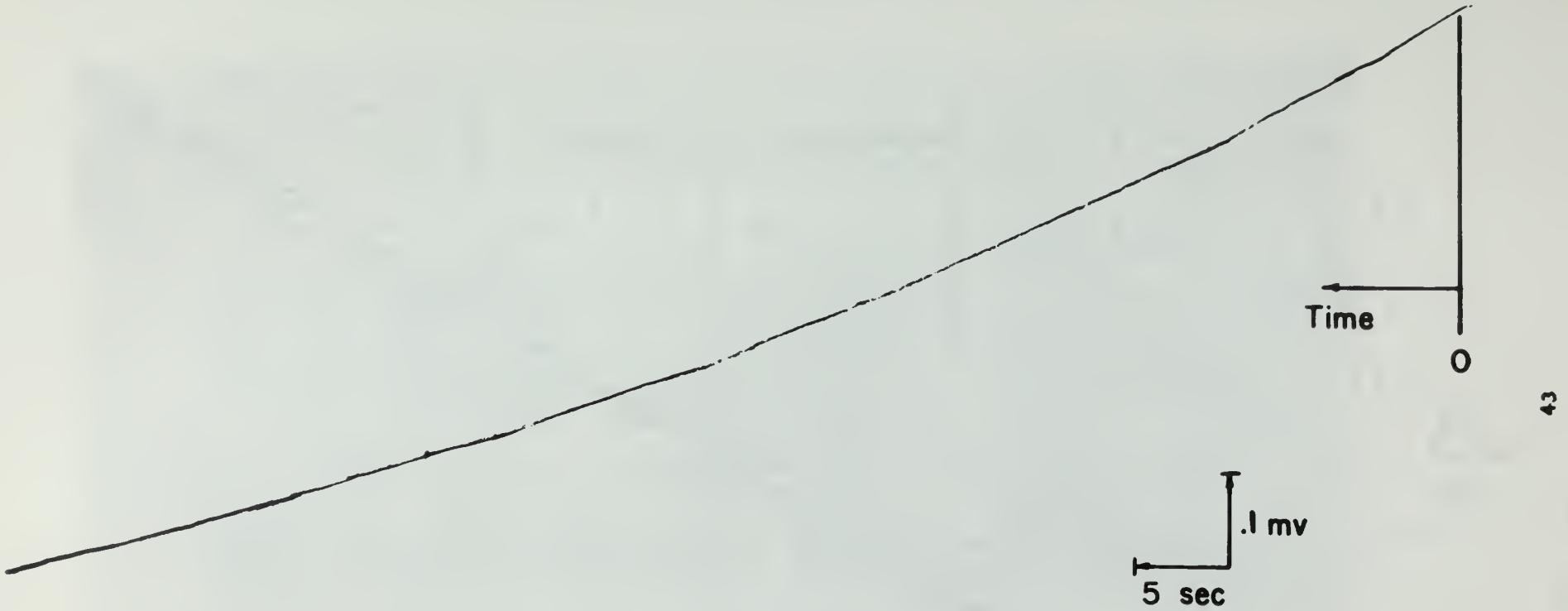

FIGURE 7. Typical Model Cooling Record

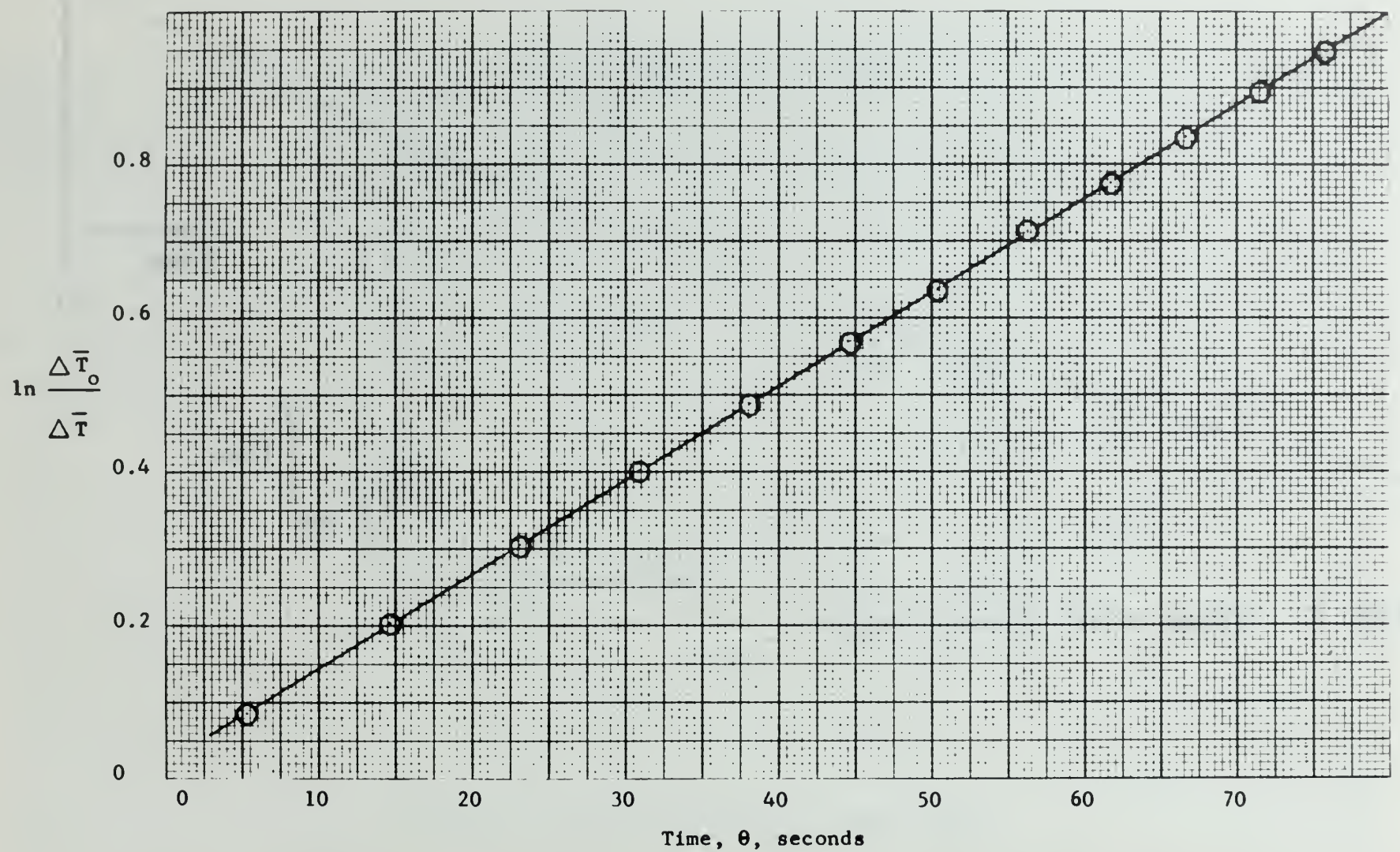

Figure 8. Plot of $\ln(\Delta \bar{T}_o / \Delta \bar{T})$ versus time for a sample run

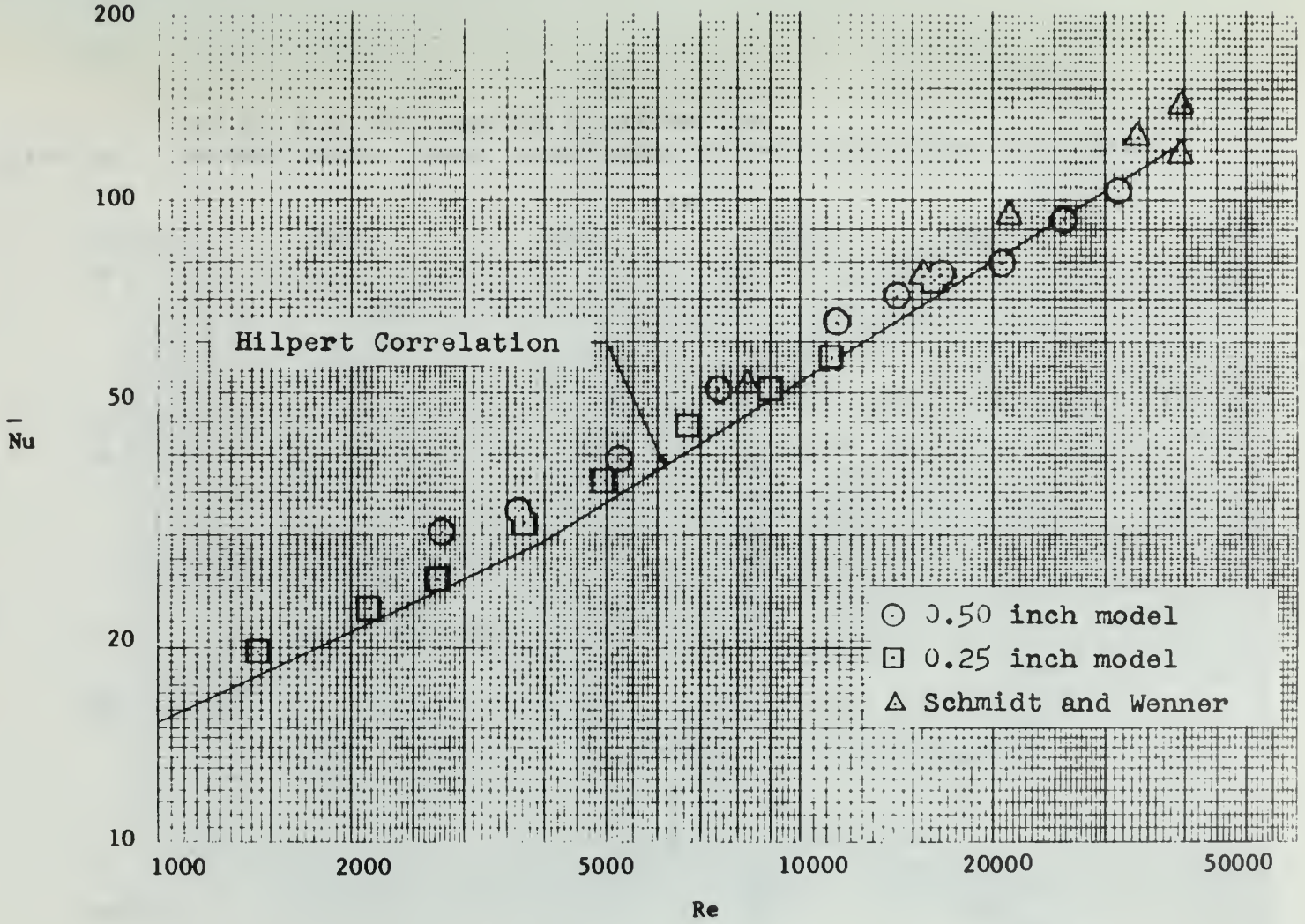

Figure 9. Summary of the normal heat transfer data for the 0.50 inch and the 0.25 inch models

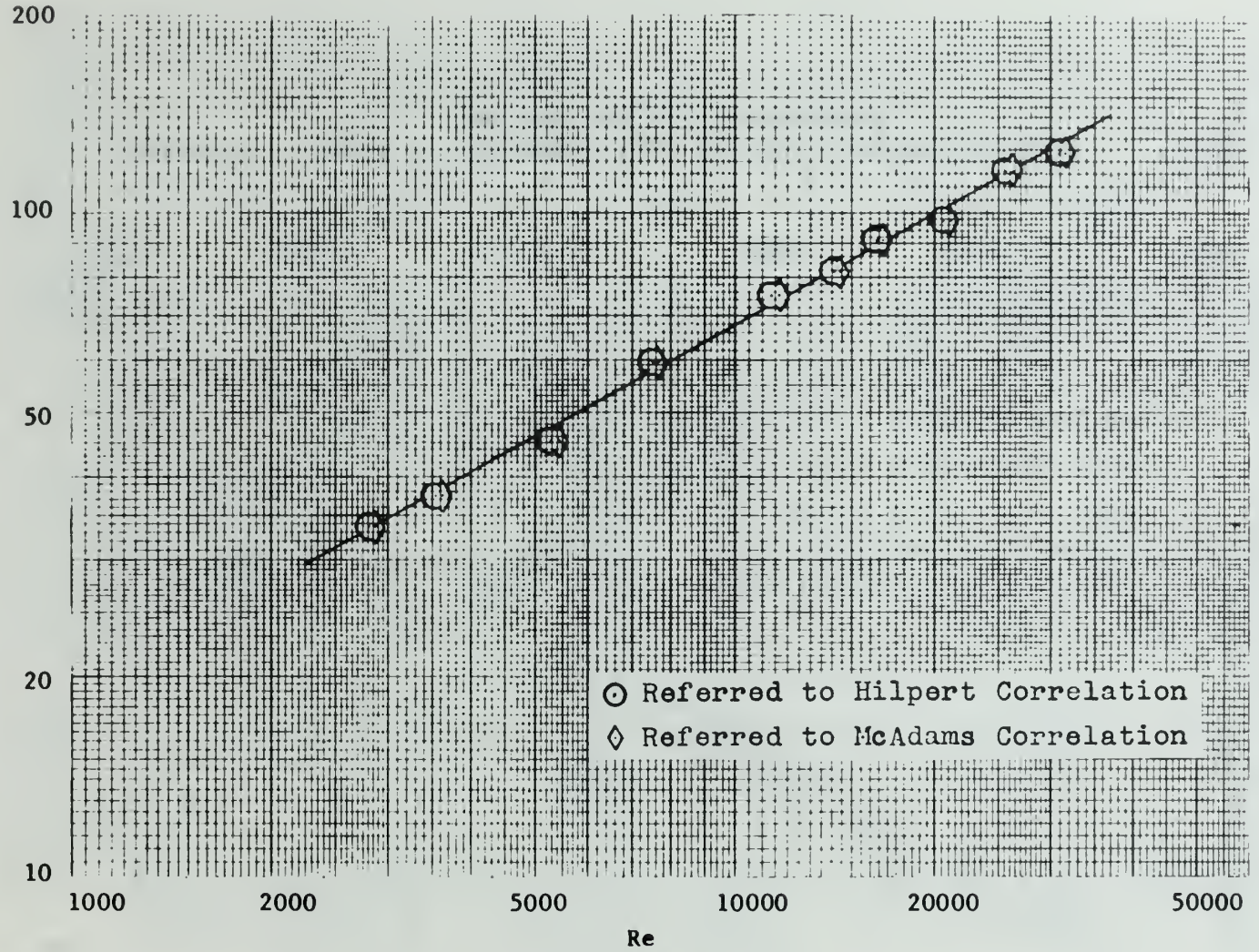

Figure 10. Average Nusselt number versus Reynolds number correlated in two ways for the 0.50 inch model at 20 degrees yaw.

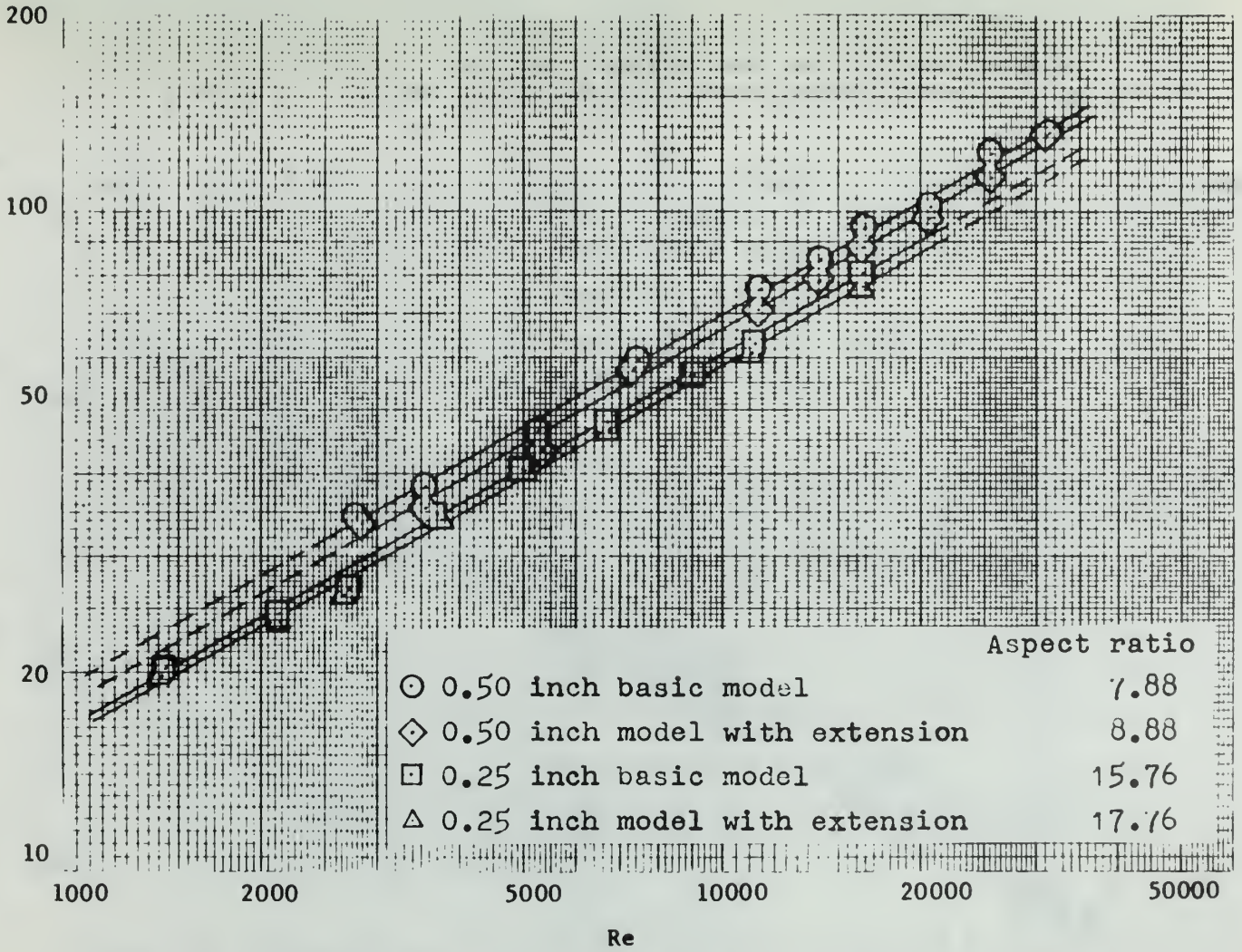

Figure 11. Average Nusselt number versus Reynolds number at 30 degrees for the 0.50 inch and the 0.25 inch models.

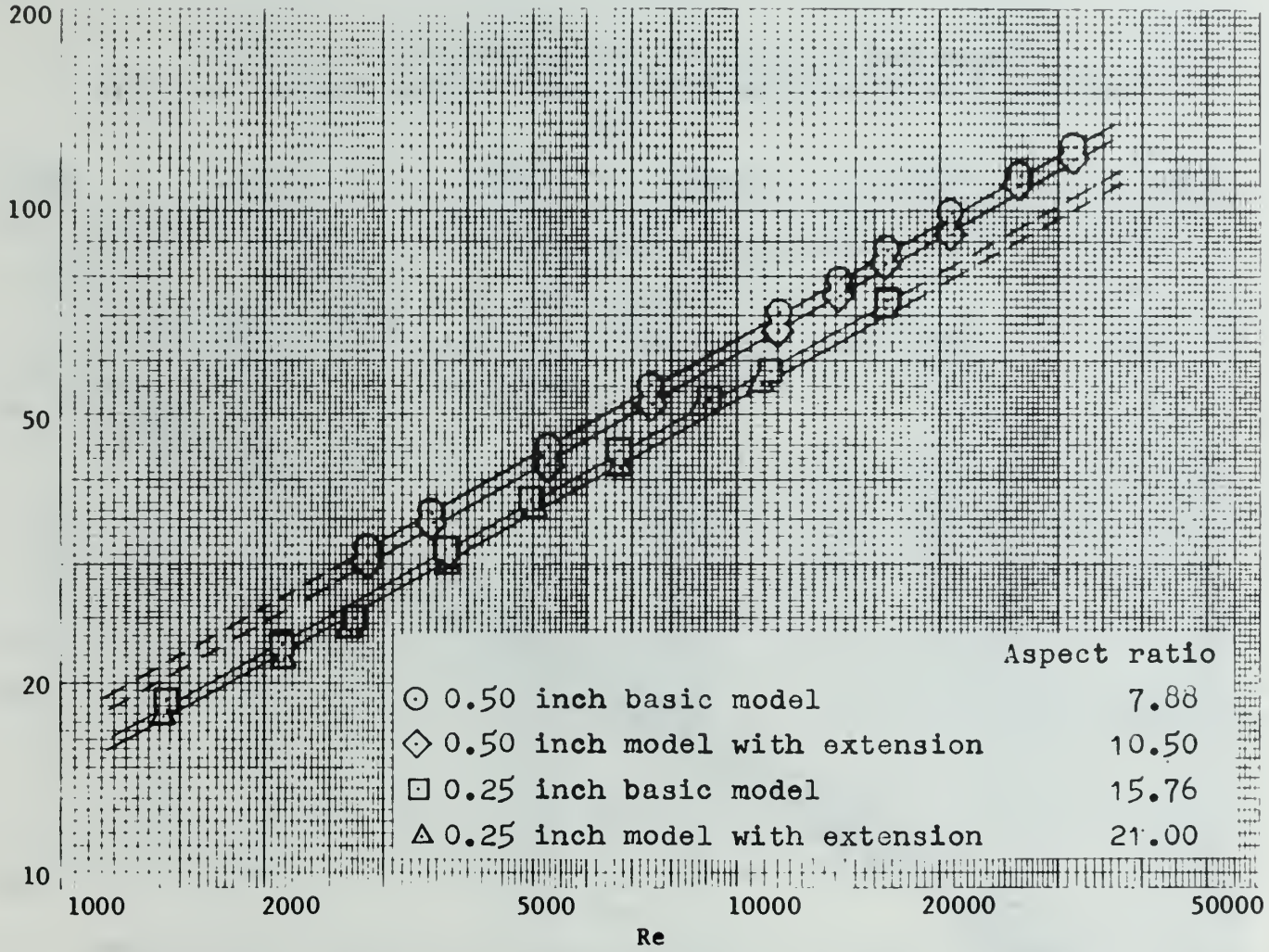

Figure 12. Average Nusselt number versus Reynolds number at 50 degrees for the 0.50 inch and the 0.25 inch models.

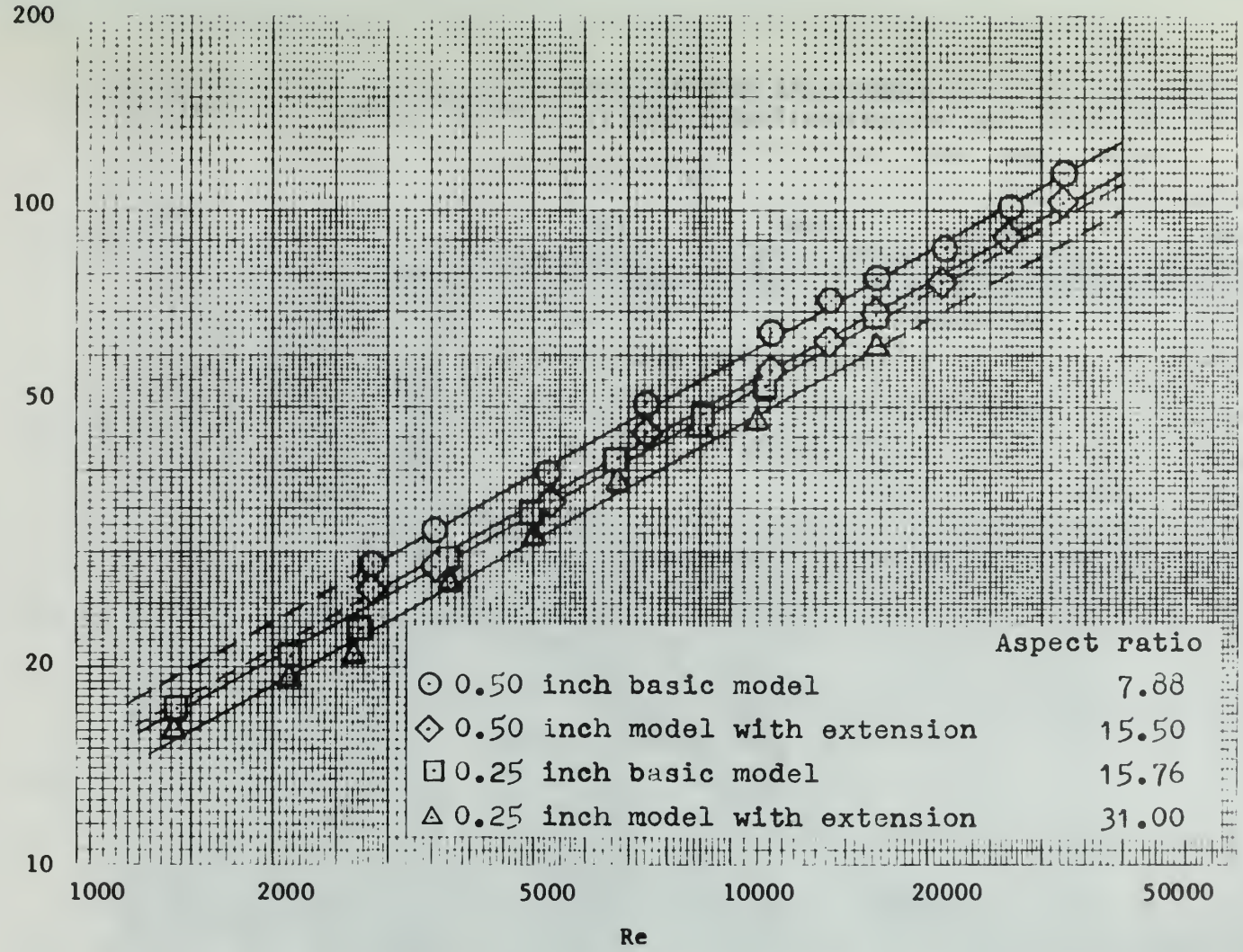

Figure 13. Average Nusselt number versus Reynolds number at 60 degrees for the 0.50 inch and the 0.25 inch models.

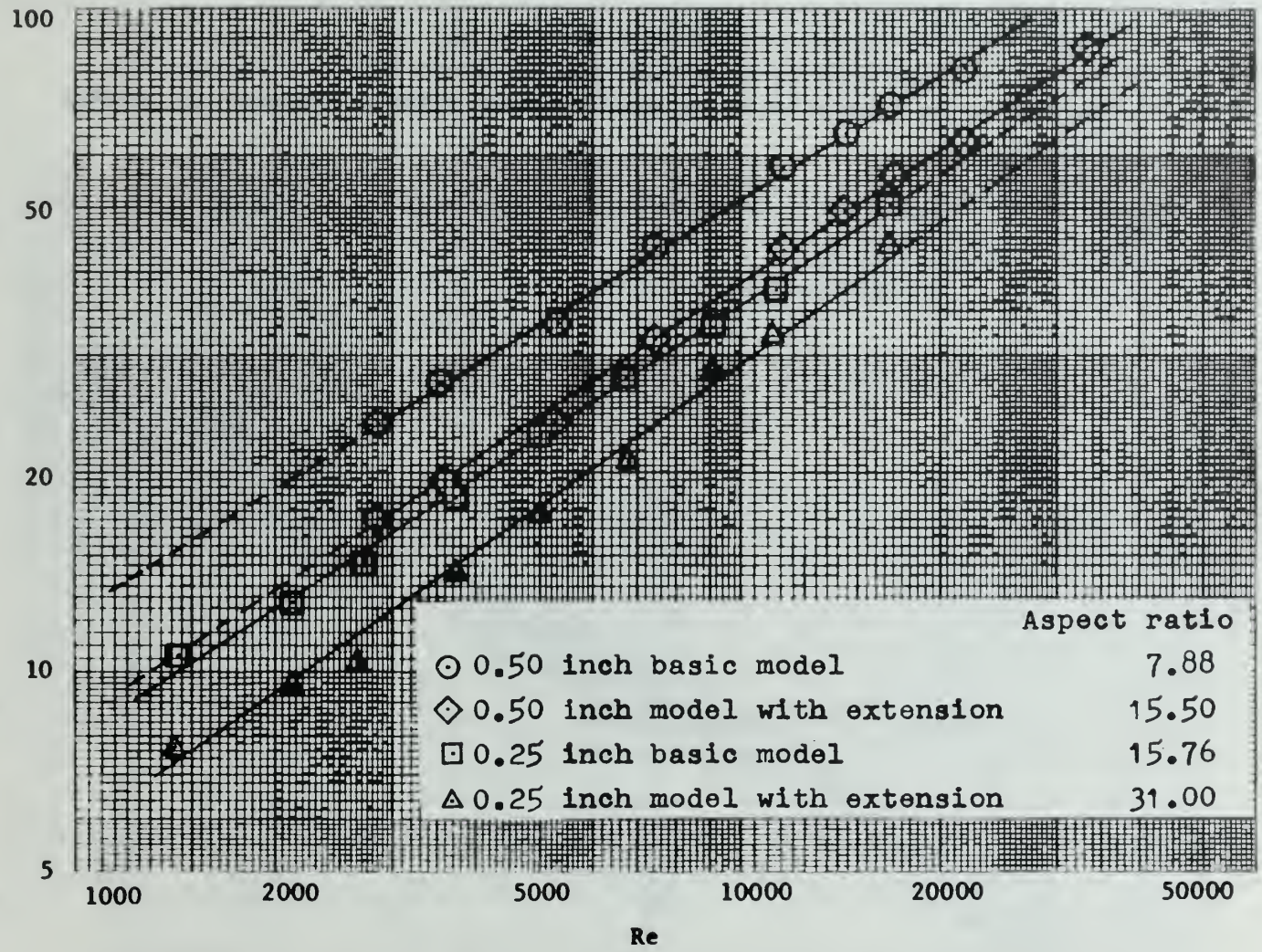

Figure 14. Summary of parallel heat transfer data for the 0.50 inch and the 0.25 inch models.

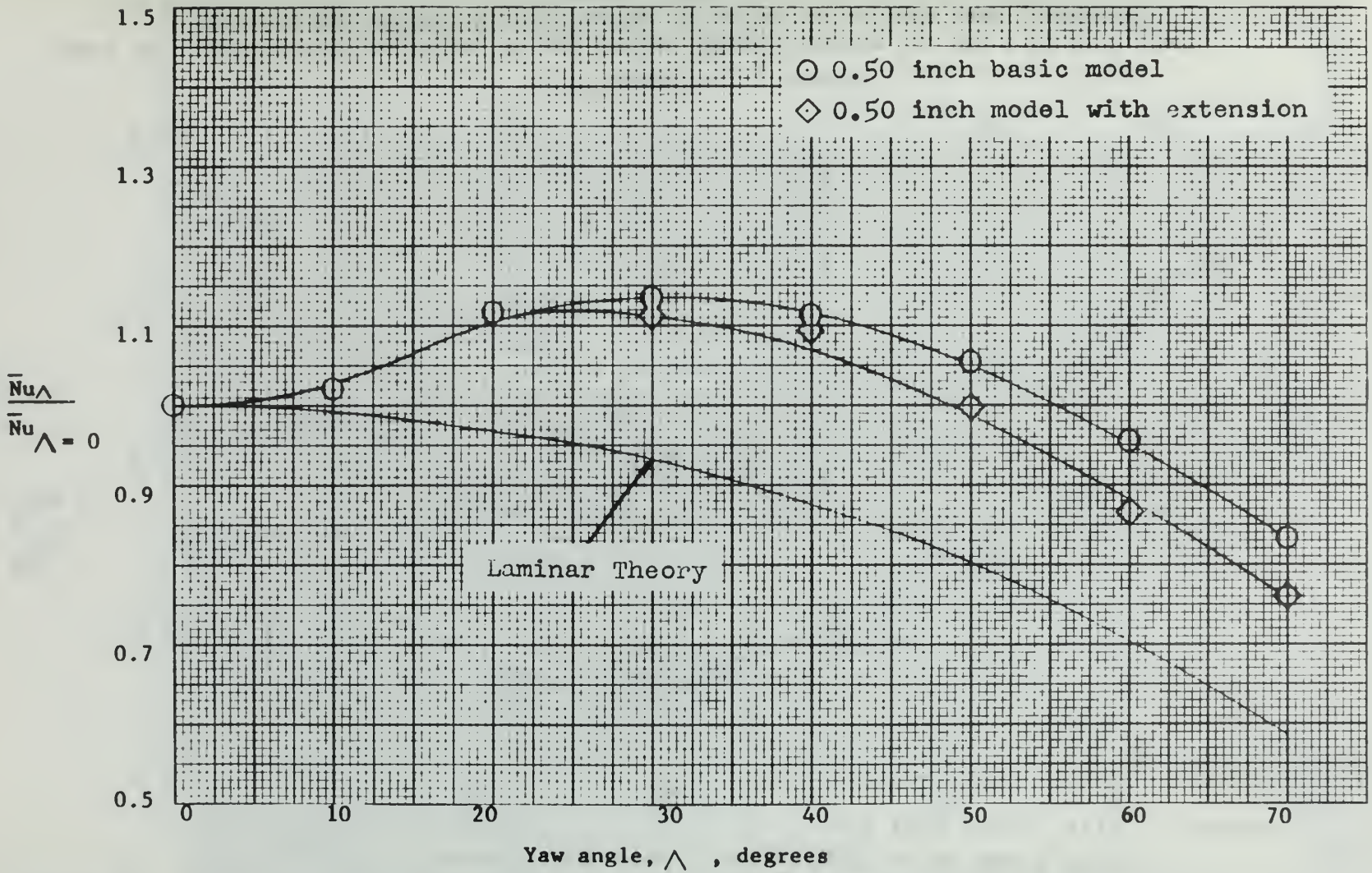

Figure 15. Experimental variation of the average Nusselt number for the 0.50 inch yawed model to the average Nusselt number of the model at zero yaw. Reynolds Number: 2800

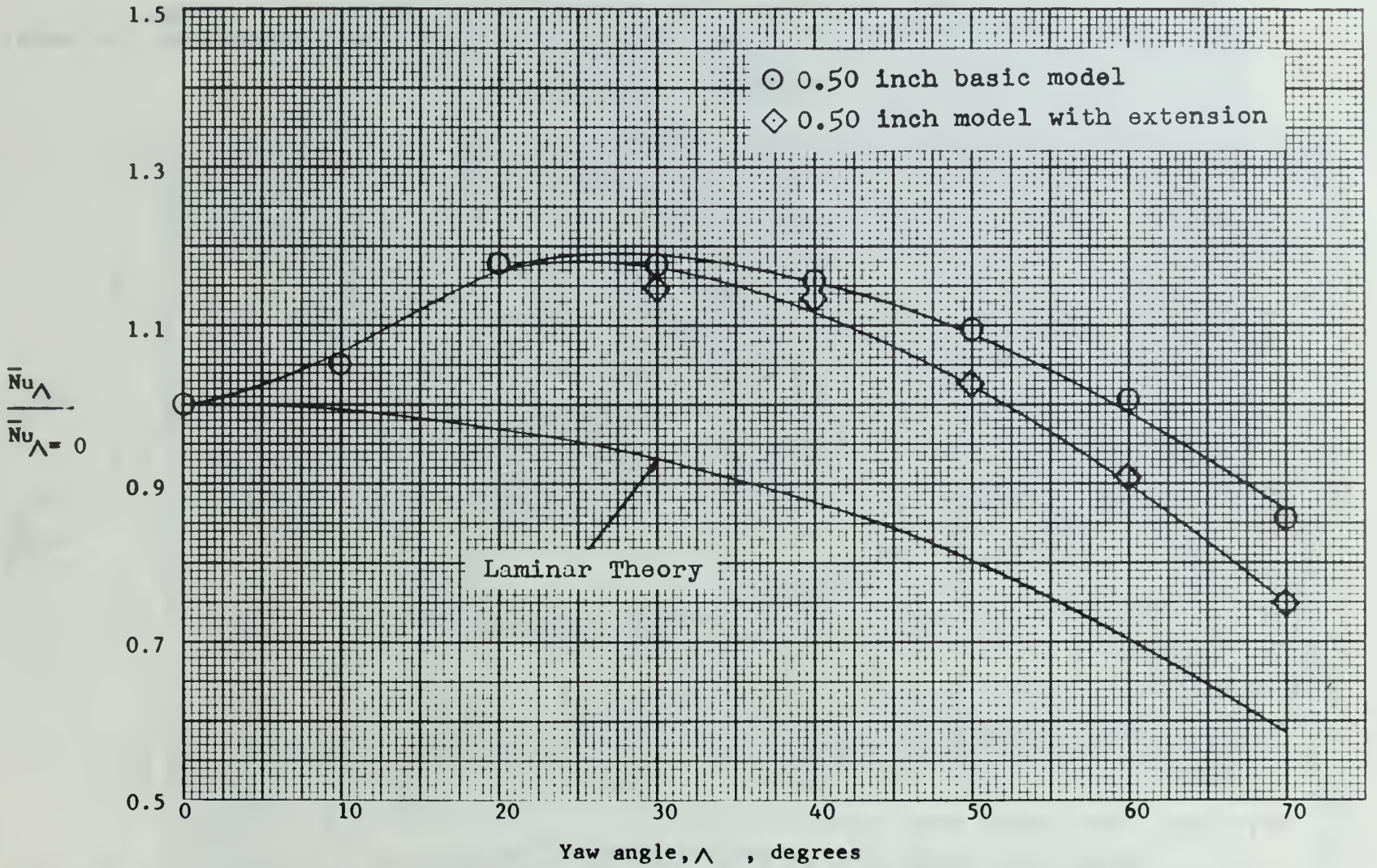

Figure 16. Experimental variation of the average Nusselt number for the 0.50 inch yawed model to the average Nusselt number of the model at zero yaw. Reynolds Number: 7460

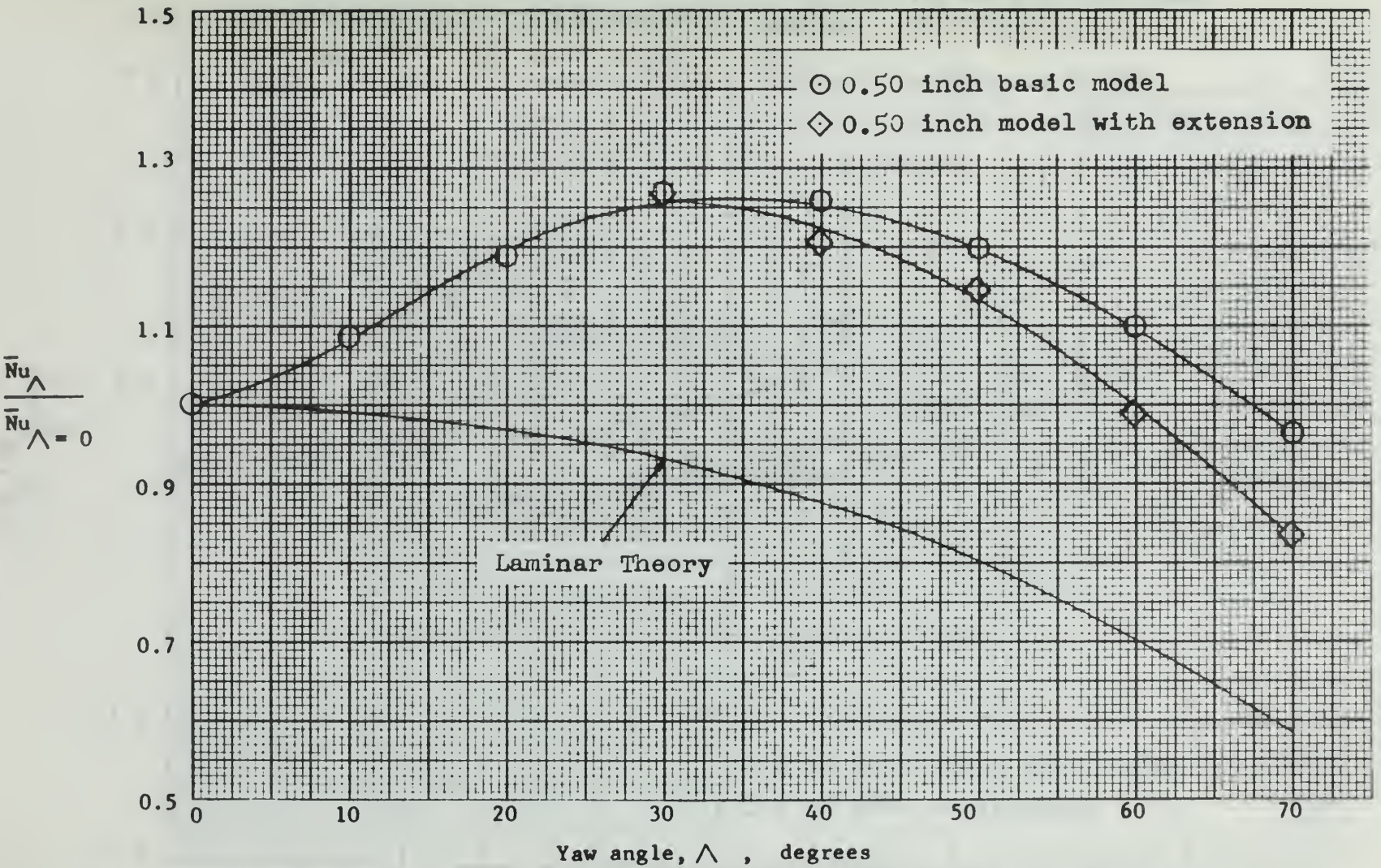

Figure 17. Experimental variation of the average Nusselt number for the 0.50 inch yawed model to the average Nusselt number of the model at zero yaw. Reynolds Number: 31900

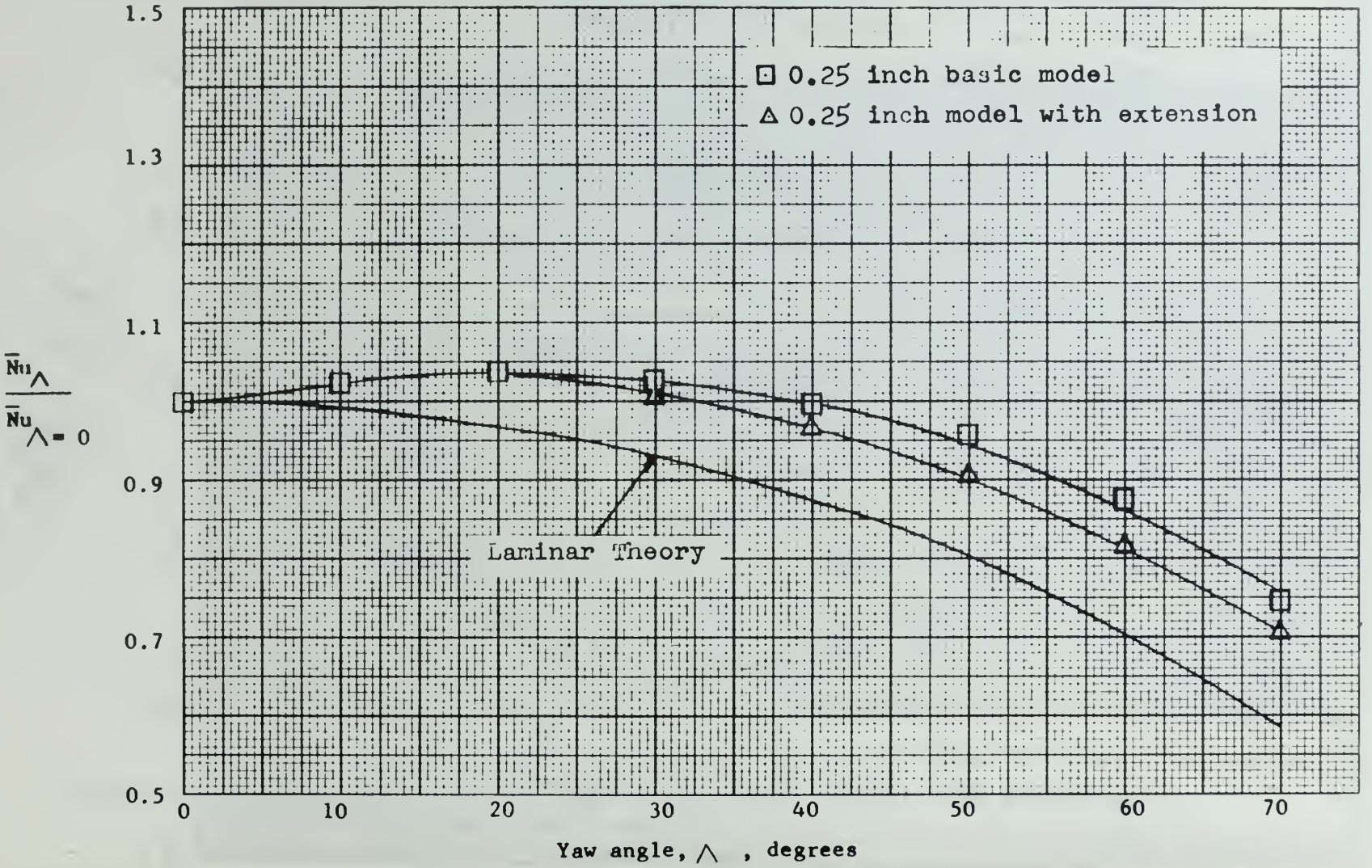

Figure 18. Experimental variation of the average Nusselt number for the 0.25 inch yawed model to the average Nusselt number of the model at zero yaw. Reynolds Number: 1460

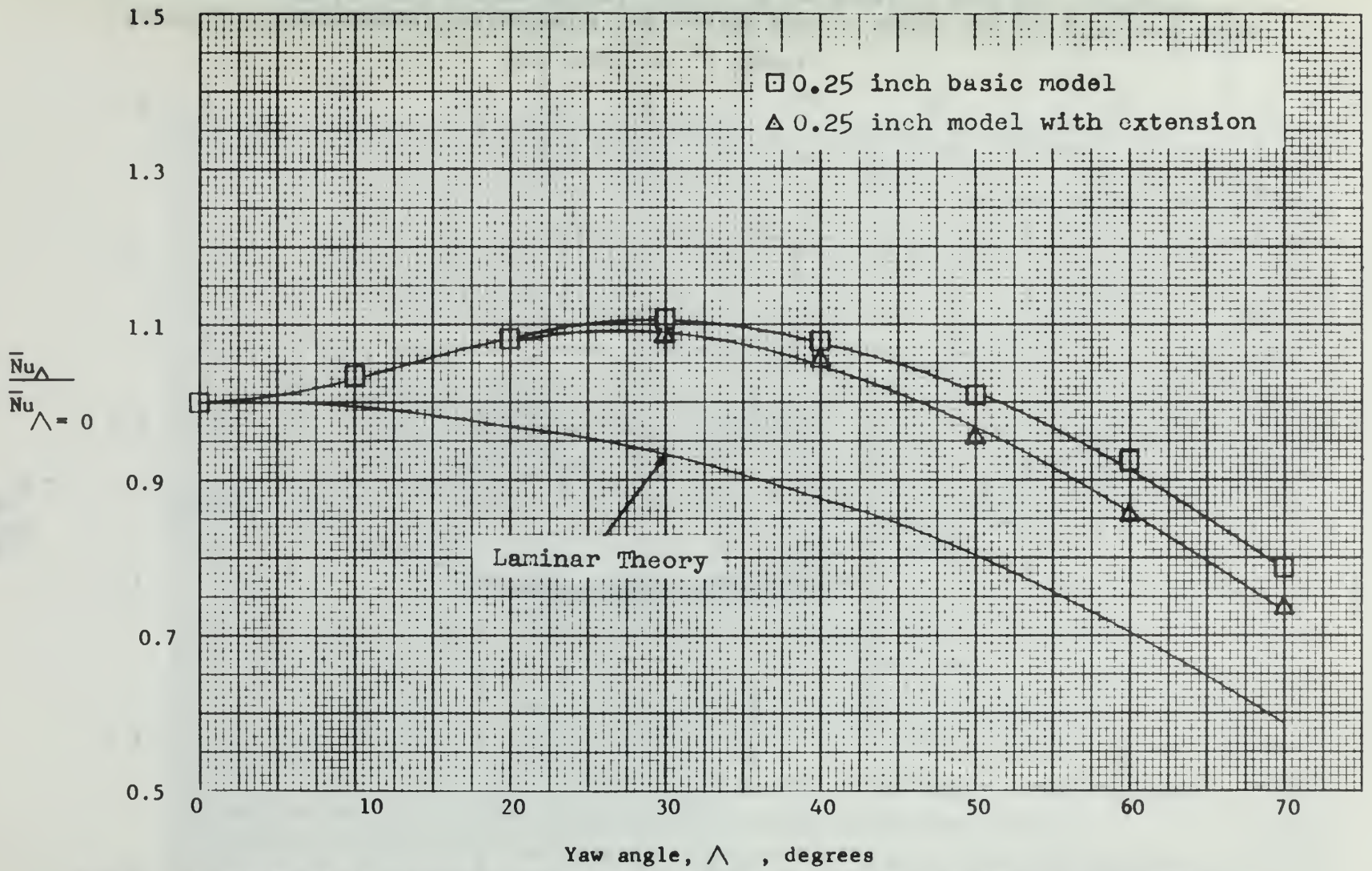

Figure 19. Experimental variation of the average Nusselt number for the 0.25 inch yawed model to the average Nusselt number of the model at zero yaw. Reynolds Number: 3720

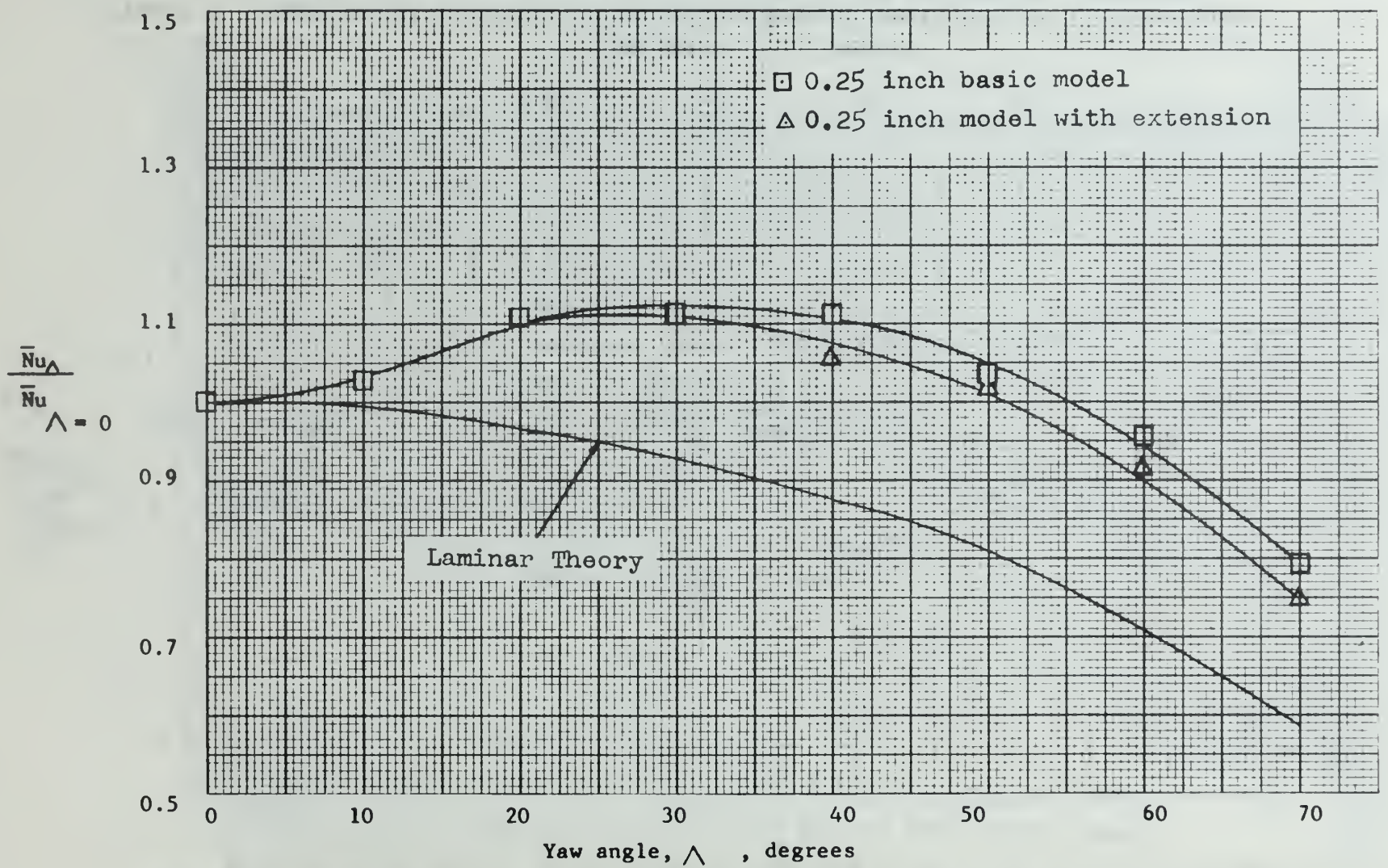

Figure 20. Experimental variation of the average Nusselt number for the 0.25 inch yawed model to the average Nusselt number of the model at zero yaw. Reynolds Number: 9050

Table I. Data of Test Models

Basic Models

Diameter	D	in	0.50	0.25
Length	L	in	0.75	0.75
Mass	m	lbm	0.04755	0.01188
Basic Length	L_a	in	3.94	3.94
Aspect ratio	L_a/D		7.88	15.76

Aspect Ratio L_a/D of Models with the Extensions for the Yaw Angles Tested

Yaw Angle	30-40	50	60-90
Total Length	4.44	5.25	7.75
Aspect ratio of the 0.50 inch model	8.88	10.50	15.50
Aspect ratio of the 0.25 inch model	17.76	21.00	31.00

Table II. Properties of Copper and Bakelite

Material	Density	Specific Heat	Thermal Conductivity	Thermal Diffusivity
	lbm/ft^3	Btu/lbm°F	Btu/hr ft°F	ft^2/hr
Copper	559	0.0918	223	4.353
Bakelite	79.5	0.40	0.1088	0.0034

Properties of pure electrolitic copper were taken from Eckert [17]. The specific heat was estimated for $\bar{t}_w = 90°F$.

Properties of bakelite were taken from the Modern Plastics Encyclopedia [20].

Table III. Summary of Heat Transfer Data for the 0.50 Inch Diameter Model

Basic Model

Yaw Angle = 0 degrees
(Normal case)

Reynolds Number	Average Nusselt Number
2753	30.3
3654	32.8
5264	39.4
7461	50.4
11487	64.2
14137	70.6
16531	76.3
20671	79.5
25932	93.3
31380	104.3

Yaw Angle = 10 degrees

2749	30.8
3579	37.6
5265	40.6
7462	52.9
11420	64.5
14042	75.0
16448	77.7
20463	87.6
25486	97.6
30909	112.9

Yaw Angle = 20 degrees

2802	33.7
3543	37.5
5290	45.1
7463	59.4
11418	75.1
14043	81.8
16363	91.0
20530	97.7
25596	115.9
30909	124.0

Table III. (Cont)

Yaw Angle = 30 degrees

Basic Model		Model with extension	
Re	$\bar{Nu}$	Re	$\bar{Nu}$
2797	34.3	2849	33.6
3542	38.1	3546	35.6
5290	46.7	5321	43.7
7463	59.4	7358	57.7
11399	76.0	11391	70.3
14091	84.4	14033	78.6
16448	94.7	16491	88.2
20726	102.3	20644	97.5
25707	122.8	25644	115.6
31211	132.3	31003	132.1
	Yaw Angle = 40 degrees		
2804	33.6	2848	33.0
3542	37.9	3546	36.1
5290	46.7	5296	45.0
7463	58.2	7465	57.1
11401	75.8	11449	72.8
14091	83.8	14150	81.8
16531	93.7	16449	88.6
20790	103.4	20900	100.9
25971	122.3	25802	117.7
31384	131.3	31132	125.7
	Yaw Angle = 50 degrees		
2846	31.8	2846	30.1
3542	35.7	3548	34.4
5290	44.6	5306	41.9
7463	55.1	7465	51.5
11517	70.6	11508	66.4
14188	79.1	14176	74.4
16655	87.3	16521	83.4
20920	98.7	20837	92.0
26439	113.3	26220	109.5
31861	124.9	31562	119.2
	Yaw Angle = 60 degrees		
2846	28.8	2845	26.2
3542	32.3	3548	28.3
5290	39.5	5302	35.9
7462	50.6	7465	45.7
11517	65.0	11509	56.5
14280	72.7	14176	62.9
16771	78.6	16655	69.9
21298	87.2	21090	77.5
26796	101.1	26527	90.3
32280	114.6	32166	102.8

Table III. (Cont)

Yaw Angle = 70 degrees

Basic Model		Model with extension	
Re	$\bar{N}u$	Re	$\bar{N}u$
2846	25.2	2845	23.0
3543	28.3	3549	26.7
5315	34.0	5302	33.7
7461	43.0	7466	37.8
11572	55.6	11581	50.1
14376	62.5	14329	55.6
16858	67.9	16777	56.8
21500	77.2	21337	68.2
27000	91.4	26830	83.1
32934	100.3	32830	86.9

Yaw Angle = 80 degrees

2849	22.0	2845	18.4
3543	24.2	3553	21.1
5326	30.4	5302	24.6
7461	39.0	7466	29.1
11566	49.3	11643	38.8
14388	56.0	14364	43.0
16934	61.7	16898	49.4
21587	69.0	21548	55.1
27347	83.7	27427	65.0
33110	95.3	33075	74.5

Yaw Angle = 90 degrees
(Parallel case)

2849	23.6	2848	17.0
3548	27.3	3590	19.4
5326	33.5	5287	23.7
7466	43.5	7461	31.8
11569	57.8	11609	43.0
14364	64.6	14310	49.3
16934	71.8	17018	55.8
21838	81.9	21591	62.5
27222	97.7	27180	75.9
33120	110.4	33214	87.2

Table IV. Summary of Heat Transfer Data for the 0.25 Inch Diameter Model

Basic Model

Yaw Angle = 0 degrees
(Normal case)

Reynolds Number	Average Nusselt Number
1435	19.7
2140	23.0
2727	25.6
3703	31.4
4991	36.6
6722	44.1
9001	50.6
11203	56.9
16203	74.9

Yaw Angle = 10 degrees

1435	20.1
2140	23.9
2727	26.1
3703	32.4
4984	37.7
6722	44.2
9001	52.1
11129	59.0
16441	76.9

Yaw Angle = 20 degrees

1435	20.4
2124	24.6
2727	27.0
3703	33.9
4978	39.9
6722	46.9
9019	56.1
11183	61.1
16444	79.8

Table IV. (cont)

Basic Model		Model with extension	
Re	$\overline{Nu}$	Re	$\overline{Nu}$
	Yaw Angle = 30 degrees		
1435	20.2	1415	19.8
2124	24.5	2145	23.9
2727	26.9	2684	26.2
3703	34.7	3740	34.0
4978	40.6	5028	40.5
6697	47.9	6751	46.5
9019	56.2	8975	56.4
11220	63.1	11058	60.8
16394	80.4	16465	77.0
	Yaw Angle = 40 degrees		
1435	19.6	1415	19.0
2124	23.7	2145	23.4
2727	26.6	2684	25.4
3703	33.5	3740	33.0
4978	40.0	5028	39.4
6697	47.2	6751	46.5
9023	56.3	8993	53.4
11127	62.2	11029	60.8
16514	78.2	16605	76.8
	Yaw Angle = 50 degrees		
1435	18.8	1415	17.8
2124	22.7	2145	21.6
2727	24.8	2684	23.8
3703	31.6	3740	29.9
4978	37.3	5028	36.0
6697	44.0	6751	41.5
9096	52.3	8975	51.6
11187	57.9	10908	55.7
16689	73.6	16605	71.8
	Yaw Angle = 60 degrees		
1435	17.2	1414	16.0
2124	20.6	2129	19.2
2727	22.8	2659	20.8
3703	29.3	3740	26.7
4991	34.2	5028	31.6
6722	41.6	6775	38.6
9111	48.5	8975	46.3
11323	53.7	10969	47.5
16729	69.2	16720	62.0

Table IV. (Cont)

Yaw Angle = 70 degrees			
Basic Model		Model with extension	
Re	$\bar{Nu}$	Re	$\bar{Nu}$
1435	14.7	1414	13.8
2124	17.3	2129	17.2
2727	19.6	2659	18.1
3712	24.7	3740	23.1
5004	29.0	5028	27.4
6722	34.3	6751	31.3
9165	40.1	9048	37.9
11360	43.2	11089	41.8
16827	58.5	16779	55.3
Yaw Angle = 80 degrees			
1435	11.7	1414	10.4
2124	13.6	2129	12.3
2727	15.7	2659	13.4
3721	18.6	3740	17.5
5004	22.6	5028	20.2
6771	26.1	6800	24.5
9147	31.9	9085	29.9
11447	37.3	11148	32.9
16729	43.6	16760	42.4
Yaw Angle = 90 degrees (Parallel case)			
1435	10.6	1414	7.7
2124	12.7	2129	9.5
2727	14.7	2671	10.3
3721	18.3	3740	14.1
5011	22.6	5028	17.3
6746	27.8	6800	20.7
9165	33.0	9103	28.3
11476	37.5	11206	32.0
16803	50.9	16703	44.0

Table V. Uncertainties for Representative runs of the 0.50 inch Diameter Model

Quantity	Value	Uncertainty	$(\frac{\Delta x}{x})\ 10^{-2}$
	RUN: B5		
T_∞	529.7	0.1	0.019
p_d	0.047	0.001	2.13
P	2098.85	0.052	0.002
T_f	542.0	0.1	0.018
k	0.4226×10^{-5}	0.0001×10^{-5}	0.024
μ	1.2441×10^{-5}	0.0002×10^{-5}	0.016
Slope	0.00722	0.00005	0.69
U_∞	14.6	0.2	1.06
Re_H	3542	38	1.06
$\bar{N}u$	37.9	0.3	0.69
	RUN: E1		
T_∞	529.9	0.1	0.019
p_d	0.485	0.010	2.060
P	2094.01	0.104	0.005
T_f	542.2	0.1	0.018
k	0.4227×10^{-5}	0.0001×10^{-5}	0.024
μ	1.2444×10^{-5}	0.0002×10^{-5}	0.016
Slope	0.0122	0.0004	3.28
U_∞	47.3	0.5	1.03
Re_H	11487	118	1.03
$\bar{N}u$	64.2	2.1	3.28

Table V. (Cont)

RUN: I12

Quantity	Value	Uncertainty	$(\frac{\Delta x}{x})10^{-2}$
T_∞	529.3	0.1	0.019
p_d	2.47	0.030	1.215
P	2114.82	0.312	0.015
T_f	541.7	0.1	0.018
k	0.4224×10^{-5}	0.0001×10^{-5}	0.024
μ	1.2436×10^{-5}	0.0002×10^{-5}	0.016
Slope	0.0224	0.0016	0.71
U_∞	105.1	0.6	0.61
Re_H	25802	157	0.61
$\bar{N}u$	117.7	8.4	7.14

Table VI. Uncertainties for Representative Runs of the 0.25 inch Diameter Model

Quantity	Value	Uncertainty	$\left(\frac{\Delta x}{x}\right) 10^{-2}$
RUN: A3			
T_∞	530.8	0.1	0.019
p_d	0.031	0.001	3.226
P	2106.03	0.052	0.002
T_f	543.1	0.1	0.018
k	0.4234×10^{-5}	0.0001×10^{-5}	0.024
μ	1.2460×10^{-5}	0.0002×10^{-5}	0.016
Slope	0.01562	0.00014	0.90
U_∞	11.8	0.2	1.61
Re_H	1435	23	1.61
$\bar{N}u$	20.4	0.2	0.90
RUN: E5			
T_∞	531.4	0.1	0.019
p_d	0.375	0.01	2.670
P	2099.26	0.104	0.005
T_f	543.7	0.1	0.018
k	0.4238×10^{-5}	0.0001×10^{-5}	0.024
μ	1.2470×10^{-5}	0.0002×10^{-5}	0.016
Slope	0.03056	0.00136	4.45
U_∞	41.2	0.6	1.34
Re_H	4978	67	1.34
$\bar{N}u$	40.0	1.8	4.45

Table VI. (Cont)

RUN: I7

Quantity	Value	Uncertainty	$(\frac{\Delta x}{x})\ 10^{-2}$
T_∞	528.6	0.1	0.019
P_d	4.20	0.08	1.905
P	2082.93	0.52	0.025
T_f	540.4	0.1	0.018
k	0.4215×10^{-5}	0.0001×10^{-5}	0.024
μ	1.2413×10^{-5}	0.0002×10^{-5}	0.016
Slope	0.05266	0.0024	4.56
U_∞	138.0	1.3	0.95
Re_H	16729	159	0.95
$\bar{N}u$	69.2	3.2	4.56

APPENDIX A

Data Reduction

Pure electrolytic copper was selected as the material of the model because its high thermal conductivity results in an interior thermal conductance which is large in comparison with the exterior convective thermal conductance. The interior temperature of the model may be taken as uniform at any instant. This is the case of negligible internal resistance in which the Biot number, the ratio of the internal thermal resistance of the body to the external resistance of its surface, is very small.

The Biot number $$Bi = \frac{h \quad D}{k_m} \tag{A-1}$$

For this case:

$$k_m \gg h \text{ and } Bi \to 0$$

An energy balance during cooling of the model yields:

$$\bar{h}_o A_s (\bar{T} - T_\infty) = - mc \frac{d\bar{T}}{d\theta} \tag{A-2}$$

that is, the rate of energy leaving the model is equal to the rate of change of internal energy of the model. Here $\bar{h}_o$ represents the combined surface conductance due to convection and radiation,

$$\bar{h}_o = \bar{h}_c + \bar{h}_r \tag{A-3}$$

where $\bar{h}_c$ is the convective heat transfer coefficient and $\bar{h}_r$ is the effective radiation heat transfer coefficient. Because of the low emissivity of the polished copper model, $\bar{h}_r$ is less than one percent of $\bar{h}_c$ and can be neglected. (See Appendix B).

The energy balance neglects axial heat conduction. The two copper cylinders located at the sides of the model proper provide thermal potentials equal to that of the model, hence, only the capacitance of the

small insulating separator cooling at a different rate will result in an axial conduction. An estimate of this amount is less than one percent and can also be neglected.

Confidence in these assumptions is obtained in the excellent agreement of the present data for the normal (unyawed) position with the results of previous investigators.

Neglecting the conduction and radiation terms, equation (A-1) can be expressed as:

$$\frac{d(\bar{T} - T_\infty)}{\bar{T} - T_\infty} = - \frac{\bar{h} A_s}{m c} d\theta \qquad \text{(A-4)}$$

If the model temperature is $\bar{T}_o$ at time θ and 0, integration of the above equation yields the following expression for the temperature-time history of the body:

$$\frac{\bar{T}_o - T_\infty}{\bar{T} - T_\infty} = e^{\frac{\bar{h} A_s}{m c} \theta} \quad \text{or} \quad \ln \frac{\bar{T}_o - T_\infty}{\bar{T} - T_\infty} = \frac{\bar{h} A_s}{m c} \theta \qquad \text{(A-5)}$$

The slope of plot $\ln \frac{\bar{T}_o - T_\infty}{\bar{T} - T_\infty}$ versus θ will be:

$$\text{slope} = \frac{\bar{h} A_s}{m c} \qquad \text{(A-6)}$$

so that the average heat transfer coefficient:

$$\bar{h} = \text{slope} \times \frac{m c}{A_s} \qquad \text{(A-7)}$$

The mass of the model was determined in a Mettler type H analytic balance. This checks closely with the determination of the mass by the product of the volume of the model times the density for pure electrolytic copper. The diameter of the model was measured before and after

assembly with the other cylinders. The mass of the model after machined down to the final size and polished was determined from the relation

$$m = m_b \left(\frac{D}{D_b} \right)^2 \qquad \text{(A-8)}$$

The properties for copper and bakelite are given in Table II.

From the model cooling curve, the times corresponding to each 0.05 millivolt decrease in thermocouple output were taken and a plot $\ln \left(\frac{\bar{T}_o - T_\infty}{\bar{T} - T_\infty} \right)$ versus θ was made. Figure 8 shows one of such for a typical run.

The best line was then drawn through the experimental points corresponding to a thermocouple output, from 0.8 to 0.4 millivolts.

Evaluation of the Film Temperature

As mentioned by Baldwin [4], for continuum flow an increase in body temperature causes an increase in the heat transfer coefficient. This effect led to the use of the "film temperature T_f" for evaluating properties in engineering correlations. The film temperature is defined as:

$$T_f = \frac{T_\infty + \bar{T}_w}{2} \qquad \text{(A-9)}$$

where T_∞ is the free stream temperature indicated for each run by the potentiometer and $\bar{T}_w$ is the average wall temperature of the model or

$$\bar{T}_w = \frac{\bar{T}_{w_{in}} + \bar{T}_{w_{fin}}}{2}$$

The initial wall temperature $\bar{T}_{w_{in}}$ was taken to be that corresponding to a temperature difference between the model and the free stream that produces 0.8 millivolt of thermocouple output. Similarly the final wall temperature $\bar{T}_{w_{fin}}$ was taken for a thermocouple output of 0.4 millivolt. In this way, the slope, film temperature and pressure measurements were evaluated at a temperature difference between the model and free stream corresponding to about 0.6 millivolt of thermocouple output.

Evaluation of the Air Density

The free stream density ρ_∞ was evaluated from the perfect gas equation:

$$\rho_\infty = \frac{P}{R\ T_\infty} \tag{A-10}$$

where P is the absolute upstream static pressure evaluated from the manometric reading from a pressure tap located at station No. 1 of the test section and the atmospheric pressure indicated by the barometer.

The film air density was evaluated similarly but using the film temperature defined by equation (A-9).

Evaluation of the Air Velocity

The air velocity was computed from the dynamic pressure indicated by the manometer connected to the pitot-static tube at the upstream station of the test section. Bernoulli's equation for a streamline

$$P + \frac{\rho\ U_\infty^2}{2} = P_s \tag{A-11}$$

from which

$$U_\infty = K_1 \left(\frac{P_d}{\rho_\infty} \right)^{0.5} \tag{A-12}$$

Evaluation of the Reynolds Number

The Reynolds number is defined as

$$R_e = \frac{U\ D\ \rho}{\mu} \tag{A-13}$$

It was evaluated in two ways. First using the free stream density ρ_∞ after McAdams [10]. Second using the film air density ρ_f, after Hilpert (cited by McAdams). The difference between these two ways of evaluation of the Reynolds number was discussed by Collins and Williams

[16]. For the present tests this amounts to a difference in Reynolds number of about two percent. Figure 10 shows the experimental points obtained for the 0.50 inches model at yaw angle of 20 degrees using both ways of correlation for the Reynolds number. All the results given are for the second form of evaluation, i.e., using film density. The viscosity and thermal conductivity of air were evaluated from the NBS Bulletin [18], at the film temperature.

Evaluation of the Average Nusselt Number

The average Nusselt number is the average heat transfer in non-dimensional form

$$\bar{N}u = \frac{\bar{h}\, D}{k} \qquad \text{(A-14)}$$

where k is the air thermal conductivity.

APPENDIX B

Radiation

For a gray body with an emissivity ϵ , at a temperature $\bar{T}$, radiating to an isothermal enclosure at temperature T_∞ , the net radiant heat exchange is:

$$q_r = \epsilon \sigma A(\bar{T}^4 - T_\infty^4) \qquad \text{(B-1)}$$

In terms of the effective radiation heat transfer coefficient, $\bar{h}_r$:

$$q_r = \bar{h}_r A (\bar{T} - T_\infty) \qquad \text{(B-2)}$$

Thus

$$\bar{h}_r = \epsilon \sigma(\bar{T} + T_\infty) (\bar{T}^2 + T_\infty^2) \qquad \text{(B-3)}$$

Using $\bar{T}$ = 95°F = 555°R

T_∞ = 70°F = 530°R

ϵ = 0.04 (Emissivity of polished copper taken from Eckert[17])

$$\bar{h}_r = (0.04)(0.1714)(10^{-8})(555 + 530) (555^2 + 530^2)$$

$$= 0.044 \quad \text{Btu/hr ft}^2\text{°F}$$

$$= 1.22 \times 10^{-5} \quad \text{Btu/sec ft}^2 \text{ °F}$$

This is well below one percent of the average convection heat transfer coefficients obtained from the present tests.

APPENDIX C

Sample Calculations

The following sample calculations are based on data obtained for a typical run for the 0.50 inch model.

Determination of the mass of the model:

Original diameter (before assembling) $D_b = 0.563$ in

Length $L = 0.750$ in

Original mass $m_b = 27.2430$ gm

Final diameter (after finished and polished) $D = 0.501$ in

Final mass, $m = m_b \left(\frac{D}{D_b}\right)^2 = 27.243 \left(\frac{0.501}{0.563}\right)^2 = 21.573$ gm

$$= \frac{21.573}{453.16} = 0.04755 \text{ lbm}$$

Heat transfer area:

$$A_s = \pi DL = \frac{\pi (0.501)(0.750)}{144} = 0.00819 \text{ ft}^2$$

Recorded Data:

Yaw angle	$\Lambda = 0$ degrees
Recorded chart Speed	$= 0.2$ in/sec
Ambient temperature	$t_a = 70$ °F
Free stream temperature	$t_\infty = 0.830$ mv.
Dynamic pressure	$p_d = 0.495$ in-H_2O
Manometric static pressure	$p = 0.57$ in-H_2O
Barometric pressure	$p_{bar} = 29.77$ in.Hga

Determination of the Film Temperature:

$$\bar{t}_{w_{in}} = t_\infty + \Delta \bar{t}_{w_{in}} = 0.830 + 0.671 = 1.501 \text{ mv.}$$

$$\bar{t}_{w_{fin}} = t_{\infty} + \Delta \bar{t}_{w_{fin}} = 0.830 + 0.450 = 1.280 \text{ mv.}$$

From a chart millivolts versus degrees Fahrenheit prepared for Copper-Constantan thermocouples:

$$t_{\infty} = 69.9\ ^{\circ}F \qquad \bar{t}_{w_{in}} = 99.3\ ^{\circ}F \qquad \bar{t}_{w_{fin}} = 89.7\ ^{\circ}F$$

The average wall temperature: $\bar{t}_w = (\bar{t}_{w_{in}} + \bar{t}_{w_{fin}})/2$

$$\bar{t}_w = (99.3 + 89.7)/2 = 94.5\ ^{\circ}F$$

The film temperature: $t_f = (t_{\infty} + \bar{t}_w)/2 = (69.9 + 94.5)/2 = 82.2\ ^{\circ}F$

Determination of the air viscosity and thermal conductivity:

From interpolation of the NBS tables of air properties [18] at a film temperature $T_f = 542.2^{\circ}R$:

Viscosity $\mu = 1.2444 \times 10^{-5}$ lbm/ft sec

Thermal conductivity $k = 0.4227 \times 10^{-5}$ Btu/sec ft °F

Determination of the slope:

T mv.	$\frac{\Delta \bar{T}_o}{\Delta \bar{T}}$	$\ln \frac{\Delta \bar{T}_o}{\Delta \bar{T}}$	θ sec
1.00	1.000	0	0
0.95	1.053	0.051	4.2
0.90	1.111	0.105	8.5
0.85	1.177	0.163	13.4
0.80	1.250	0.223	18.3
0.75	1.333	0.287	23.7
0.70	1.428	0.356	29.6
0.65	1.538	0.430	35.4
0.60	1.667	0.511	41.9
0.55	1.818	0.598	49.1
0.50	2.000	0.693	56.9
0.45	2.222	0.798	65.4
0.40	2.500	0.916	74.7
0.35	2.857	1.050	85.6
0.30	3.333	1.204	98.2

Figure 8 is the plot $\ln \frac{\Delta \bar{T}_o}{\Delta \bar{T}}$ versus time for this sample run.

From Figure 8,

$$\text{slope} = \frac{0.611}{50} = 0.01222 \text{ sec}^{-1}$$

Determination of the average heat transfer coefficient:

$$\bar{h} = \text{slope} \frac{m\ c}{A_s} = 0.01222 \frac{(0.04755)\ (0.0918)}{0.00819} = 0.00650 \text{ Btu/sec ft}^2.$$

Determination of the average Nusselt Number:

$$\overline{Nu} = \frac{\bar{h}\, D}{k} = \frac{(0.00650)\ (0.501)}{12\ (0.4227 \times 10^{-5})} = 64.2$$

Determination of the density:

$$P_{atm} = P_{bar} + \text{inst.corr.} = 29.77 + (-0.13) = 29.64 \text{ in.Hga}$$

$$P = P_{atm} - p = 13.6 \times 29.64 - 0.57 = 402.534 \text{ in-}H_2O$$

$$P = \frac{(402.534)\ (12)\ (14.696)}{33.9} = 2094.03 \text{ lbf/ft}^2$$

$$\rho_\infty = \frac{2094.03}{(53.35)\ (529.9)} = 0.0741 \text{ lbm/ft}^3$$

$$\rho_f = \frac{2094.03}{(53.35)\ (542.2)} = 0.0724 \text{ lbm/ft}^3$$

Determination of the free stream velocity:

$$U_\infty = [2/\rho_\infty\ (P_s - P)]^{0.5} = \left[\frac{2\ (14.696)\ 12\ (32.174)}{33.9}\right]^{0.5} (p_d/\rho_\infty)^{0.5}$$

$$= 18.2961\ (p_d/\rho_\infty)^{0.5}$$

$$= 18.2961\ \left(\frac{0.495}{0.0741}\right)^{0.5} = 47.29 \text{ ft/sec}$$

Evaluation of the Reynolds Number:

The Reynolds Number correlated with the free stream density after McAdams [2]

$$Re_M = (U_\infty\ D\ \rho_\infty)/\mu = \frac{(47.29)(0.501)\ (0.0741 \times 10^{-5})}{12\ (1.2444 \times 10^{-5})} = 11757$$

The Reynolds Number correlated with the free stream density after Hilpert (cited by McAdams)

$$Re_H = (U_\infty D \rho_f)/\mu = \frac{(47.29)\ (0.501)\ (0.0724 \times 10^{-5})}{12\ (1.2444 \times 10^{-5})} = 11487$$

APPENDIX D

Uncertainty Analysis

The manner in which the present tests compare with the ideal case of the heat transfer for an infinite long cylinder was discussed in Section five.

Uncertainties in physical properties:

No uncertainties were considered for the thermal properties of copper given by Eckert [17]. The values of viscosity and thermal conductivity for air given by the NBS bulletin [18] were considered correct. Their uncertainty depends only upon the film temperature at which they were evaluated. The air density was evaluated at the upstream station using the perfect gas equation. Its uncertainty depends upon the upstream static pressure and temperature. Uncertainties in the thermal properties of the air were found to be negligible.

Uncertainty in the mass and lineal dimensions of the model:

The mass of the model was determined in an analytic balance so that the uncertainty in the determination in mass is negligible. The errors in lineal dimensions are considered of the order of 0.1 percent and neglected.

Instrumentation inaccuracies:

In the determination of the uncertainties reported, the method of Kline and McClintock [19] was used assuming that all variables have a normal Gaussian distribution.

Temperature:

The free stream temperature was obtained by a calibrated copper-constantan thermocouple connected to a Leeds and Northrup portable potentiometer with an ice reference. Assuming a correct calibration of the thermocouple, the estimated possible error is $\pm$ one half of the smallest division of the potentiometer or $\pm$ 0.0025 millivolts which corresponds to 0.1 degrees Fahrenheit.

Pressure:

Since the range of pressure varied requiring different manometers the uncertainty in pressure varies for different runs. An analysis for three representative runs at different Reynolds number was made to allow an estimation of the uncertainties at low, middle and high Reynolds numbers.

Uncertainty in the Nusselt number:

The average Nusselt number $\overline{Nu} = \frac{\bar{h} D}{k}$ (D-1)

Substituting the average heat transfer coefficient from equation (A-7):

$$Nu = \frac{m c}{\pi L} \quad \frac{slope}{k} \tag{D-2}$$

The uncertainty in Nusselt number can be expressed as:

$$\frac{\Delta Nu}{Nu} \approx \frac{\Delta slope}{slope} \tag{D-3}$$

Because the uncertainties in the air thermal properties and the uncertainties in the lineal dimensions were estimated as negligible, the average Nusselt number depends mainly upon the uncertainty in the plot

$\ln(\Delta\bar{T}_o / \Delta\bar{T})$ versus time. The determination of the slope was a graphical procedure whose accuracy depended on the scale used and on the value of the slope itself. The uncertainty in the slope is greater for the faster runs when the times for cooling were small. A time scale from 0 to 200 seconds, and from 0 to 150 seconds was used for the determination of the slope of the 0.5 inches and 0.25 inches model respectively. The difference in the time scale used accounts for the small difference in the uncertainties in the slopes of the two models.

Uncertainty in the free stream velocity:

The free stream velocity can be expressed as:

$$U_\infty = K_1 \, (p_d / \rho_\infty)^{0.5} \qquad \text{(D-4)}$$

and using the perfect gas law:

$$U_\infty = K_2 \, \left(\frac{p_d \, T_\infty}{P}\right)^{0.5} \qquad \text{(D-5)}$$

where P is the upstream absolute pressure and p_d the dynamic pressure. The uncertainty in the atmospheric pressure was estimated as 0.01 in-Hg and neglected.

The expression of the uncertainty in the velocity can be written as

$$\frac{\Delta U_\infty}{U_\infty} = 1/2 \left[\left(\frac{\Delta p_d}{p_d}\right)^2 + \left(\frac{\Delta T_\infty}{T_\infty}\right)^2 + \left(\frac{\Delta P}{P}\right)^2 \right]^{0.5} \qquad \text{(D-6)}$$

The uncertainties in temperature and absolute pressure were found to be less than 0.1 percent and neglected. With this consideration the uncertainty in the velocity becomes:

$$\Delta U_\infty / U_\infty \approx \Delta p_d / 2 \, p_d \qquad \text{(D-7)}$$

depending mainly upon the uncertainty in the dynamic pressure measured with the pitot-static tube.

Uncertainty in Reynolds Number:

The Reynolds number

$$Re_H = \frac{U_\infty \, D \, \rho_f}{\mu} \qquad \text{(D-8)}$$

with the air density evaluated at the film temperature.

Introducing the free stream velocity from Equation (D-4), the Reynolds Number becomes:

$$Re_H = \frac{K_3}{\mu \, T_f} (p_d \; P \; T_\infty)^{0.5} \qquad \text{(D-9)}$$

The uncertainty in Reynolds number can be expressed as:

$$\frac{\Delta Re_H}{Re_H} = \left[\left(\frac{\Delta \mu}{\mu} \right)^2 + \left(\frac{\Delta T_f}{T_f} \right)^2 + \left(\frac{\Delta p_d}{2 \, p_d} \right)^2 + \left(\frac{\Delta P}{2 \, P} \right)^2 + \left(\frac{\Delta T_\infty}{2 \, T_\infty} \right)^2 \right]^{0.5} \qquad \text{(D-10)}$$

With the same considerations as before with respect to the uncertainties in viscosity, temperature and static pressure, the uncertainty in Reynolds number depends basically upon the uncertainty in the free stream velocity.

$$\Delta Re_H \; / \; Re_H \approx \Delta U_\infty \; / \; U_\infty \qquad \text{(D-11)}$$

Tables V and VI present an estimation of the uncertainties for representative runs of the 0.50 and the 0.25 inch model respectively.

INITIAL DISTRIBUTION LIST

		No. Copies
1.	Defense Documentation Center Cameron Station Alexandria, Virginia 22314	20
2.	Library Naval Postgraduate School Monterey, California 93940	2
3.	COMANDANCIA GENERAL DE MARINA DEPARTAMENTO DE INSTRUCCION Quito, ECUADOR	1
4.	Department of Mechanical Engineering Naval Postgraduate School Monterey, California 93940	2
5.	Prof. Paul F. Pucci Department of Mechanical Engineering Naval Postgraduate School Monterey, California 93940	3
6.	LT Marco A. Viteri, Ecuadorian Navy Primera Zona Naval Guayaquil, ECUADOR	3
7.	LT Gerardo Hiriart 615 Ocean Ave., Monterey, California 93940	1

DOCUMENT CONTROL DATA - R & D

(Security classification of title, body of abstract and indexing annotation must be entered when the overall report is classified)

1. ORIGINATING ACTIVITY *(Corporate author)*
Naval Postgraduate School
Monterey, Calif. 93940

2a. REPORT SECURITY CLASSIFICATION
Unclassified

2b. GROUP

3. REPORT TITLE
Experimental Determination of the Average Heat Transfer Coefficient for Yaw Cylinders

4. DESCRIPTIVE NOTES *(Type of report and inclusive dates)*
Thesis for Master of Science Degree, April 1969

5. AUTHOR(S) *(First name, middle initial, last name)*
Marco Antonio Viteri

6. REPORT DATE	7a. TOTAL NO. OF PAGES	7b. NO. OF REFS
April 1969	82	

8a. CONTRACT OR GRANT NO.	9a. ORIGINATOR'S REPORT NUMBER(S)
b. PROJECT NO. N/A	N/A
c.	9b. OTHER REPORT NO(S) *(Any other numbers that may be assigned this report)*
d.	N/A

10. DISTRIBUTION STATEMENT
Distribution of this document is unlimited.

11. SUPPLEMENTARY NOTES	12. SPONSORING MILITARY ACTIVITY
	Naval Postgraduate School Monterey, Calif. 93940

13. ABSTRACT

The heat transfer characteristics of yawed cylinders was measured in an open induction tunnel in the subsonic range. Two model diameters were tested, 0.50 inches and 0.25 inches. The Reynolds number based on cylinder diameter was varied from 2750 to 33200 for the 0.50 inch diameter model and from 1430 to 16700 for the 0.25 inch diameter model.

The tests showed a good agreement for both models with the experimental results of other investigators for the normal case, or zero yaw case. As yaw angle was increased from the normal position to about 35 degrees, a peaking in the heat transfer was obtained. As yaw angle was increased further the average Nusselt number decreased. This behavior is attributed to the end effect of the models used whose aspect ratio were limited by the size of the test section. At larger yaw angles there is an agreement of the heat transfer data for models with similar aspect ratio.

KEY WORDS	LINK A		LINK B		LINK C	
	ROLE	WT	ROLE	WT	ROLE	WT
Yawed cylinder forced convection						
Forced convection, yawed cylinders						
Cylinders, forced convection						